group for PC in negative-ion mode.[17] Interestingly, there was a 10-fold decrease (9.8%) in the 16:0-22:6-PC levels versus the control in *rmd* hindlimb muscle and also in muscle mitochondria (Figure 2C), indicating the importance of the PC de novo synthesis pathway for maintaining not only PC levels but also fatty acid composition of PC molecular species. Similarly, in forelimb muscle 16:0-22:6 PC levels were also decreased in comparison to the control, but to a milder extent (18.2%), suggesting an association between severity of muscle damage and fatty acid composition alteration of PC (data not shown). In *rmd* mice, it has been shown that muscle PC can be delivered from plasma lipoprotein,[18] suggesting that non-decreased PC molecular species might be derived from the plasma, whereas 16:0-22:6 PC might be synthesized only in muscle (and possibly in brain). However, confirmation of this requires further studies.

Individuals with *CHKB* mutations have severe mental retardation in addition to the muscular dystrophy. Interestingly, polymorphisms near the *CHKB* locus and decreased CHKB expression have been associated with narcolepsy with cataplexy, suggesting a link between CHK-β activity and the maintenance of normal brain function in humans.[19] Furthermore, brain damage in pneumococcal infection has been attributed to the inhibition of de novo PC synthesis, suggesting the importance of PC synthesis for the brain.[20] Our data provide evidence that altered phospholipid biosynthesis is a causative agent for a human congenital muscular dystrophy, and further studies will elucidate the detailed molecular mechanisms of the disease in both muscle and brain.

Supplemental Data

Supplemental Data include four figures and can be found with this article online at http://www.cell.com/AJHG/.

Acknowledgments

We are grateful to the patients and their family for their participation, to Megumu Ogawa, Etsuko Keduka, Yuriko Kure, Mieko Ohnishi, Kaoru Tatezawa, and Kazu Iwasawa (National Center of Neurology and Psychiatry) for their technical assistance, to Naoki Kondou and Hiroyuki Taguchi (Kao Corporation) for their kind support on mass analysis, to Osamu Fujino and Kiyoshi Takahashi (Department of Pediatrics, Nippon Medical School) for providing patient information, and to Ken Inoue (National Center of Neurology and Psychiatry) for thoughtful comments on genetics. This study was supported partly by the Research on Psychiatric and Neurological Diseases and Mental Health of Health and Labour Sciences research grants; partly by Research on Intractable Diseases of Health and Labor Sciences research grants; partly by a Research Grant for Nervous and Mental Disorders (20B-12, 20B-13) from the Ministry of Health, Labour and Welfare; partly by an Intramural Research Grant (23-4, 23-5) for Neurological and Psychiatric Disorders from NCNP; partly by KAKENHI (20390250, 22791019); partly by Research on Publicly Essential Drugs and Medical Devices of Health and Labor Sciences research grants; partly by the Program for Promotion of Fundamental Studies in Health Sciences of the National Institute of Biomedical Innovation (NIBIO); and partly by a grant from the Japan Foundation for Neuroscience and Mental Health. G.A.C. and R.B S. were supported in part by a National Institutes of Health grant (AR-49043 to G.A.C.).

Received: March 21, 2011
Revised: April 21, 2011
Accepted: May 10, 2011
Published online: June 9, 2011

Web Resources

The URLs for data presented herein are as follows:

GenBank, http://www.ncbi.nlm.nih.gov/Genbank
Online Mendelian Inheritance in Man (OMIM), http://www.omim.org
R software version 2.11.0, http://www.r-project.org/

References

1. Sher, R.B., Aoyama, C., Huebsch, K.A., Ji, S., Kerner, J., Yang, Y., Frankel, W.N., Hoppel, C.L., Wood, P.A., Vance, D.E., and Cox, G.A. (2006). A rostrocaudal muscular dystrophy caused by a defect in choline kinase beta, the first enzyme in phosphatidylcholine biosynthesis. J. Biol. Chem. *281*, 4938–4948.
2. Nishino, I., Kobayashi, O., Goto, Y., Kurihara, M., Kumagai, K., Fujita, T., Hashimoto, K., Horai, S., and Nonaka, I. (1998). A new congenital muscular dystrophy with mitochondrial structural abnormalities. Muscle Nerve *21*, 40–47.
3. Hayashi, Y.K., Matsuda, C., Ogawa, M., Goto, K., Tominaga, K., Mitsuhashi, S., Park, Y.E., Nonaka, I., Hino-Fukuyo, N., Haginoya, K., et al. (2009). Human PTRF mutations cause secondary deficiency of caveolins resulting in muscular dystrophy with generalized lipodystrophy. J. Clin. Invest. *119*, 2623–2633.
4. Liao, H., Aoyama, C., Ishidate, K., and Teraoka, H. (2006). Deletion and alanine mutation analyses for the formation of active homo- or hetero-dimer complexes of mouse choline kinase-α and -β. Biochim. Biophys. Acta *1761*, 111–120.
5. Aoyama, C., Yamazaki, N., Terada, H., and Ishidate, K. (2000). Structure and characterization of the genes for murine choline/ethanolamine kinase isozymes alpha and beta. J. Lipid Res. *41*, 452–464.
6. Ishidate, K., and Nakazawa, Y. (1992). Choline/ethanolamine kinase from rat kidney. Methods Enzymol. *209*, 121–134.
7. Matsumoto, H., Hayashi, Y.K., Kim, D.S., Ogawa, M., Murakami, T., Noguchi, S., Nonaka, I., Nakazawa, T., Matsuo, T., Futagami, S., et al. (2005). Congenital muscular dystrophy with glycosylation defects of α-dystroglycan in Japan. Neuromuscul. Disord. *15*, 342–348.
8. Mitsuhashi, H., Futai, E., Sasagawa, N., Hayashi, Y., Nishino, I., and Ishiura, S. (2008). Csk-homologous kinase interacts with SHPS-1 and enhances neurite outgrowth of PC12 cells. J. Neurochem. *105*, 101–112.
9. Aoyama, C., Liao, H., and Ishidate, K. (2004). Structure and function of choline kinase isoforms in mammalian cells. Prog. Lipid Res. *43*, 266–281.
10. Bligh, E.G., and Dyer, W.J. (1959). A rapid method of total lipid extraction and purification. Can. J. Biochem. Physiol. *37*, 911–917.
11. Rouser, G., Fkeischer, S., and Yamamoto, A. (1970). Two dimensional then layer chromatographic separation of polar

lipids and determination of phospholipids by phosphorus analysis of spots. Lipids *5*, 494–496.
12. Aoyama, C., Ohtani, A., and Ishidate, K. (2002). Expression and characterization of the active molecular forms of choline/ethanolamine kinase-α and -β in mouse tissues, including carbon tetrachloride-induced liver. Biochem. J. *363*, 777–784.
13. Wu, G., Aoyama, C., Young, S.G., and Vance, D.E. (2008). Early embryonic lethality caused by disruption of the gene for choline kinase alpha, the first enzyme in phosphatidylcholine biosynthesis. J. Biol. Chem. *283*, 1456–1462.
14. Wu, G., Sher, R.B., Cox, G.A., and Vance, D.E. (2010). Differential expression of choline kinase isoforms in skeletal muscle explains the phenotypic variability in the rostrocaudal muscular dystrophy mouse. Biochim. Biophys. Acta *1801*, 446–454.
15. Nakanishi, H., Iida, Y., Shimizu, T., and Taguchi, R. (2010). Separation and quantification of sn-1 and sn-2 fatty acid positional isomers in phosphatidylcholine by RPLC-ESIMS/MS. J. Biochem. *147*, 245–256.
16. Ikeda, K., Mutoh, M., Teraoka, N., Nakanishi, H., Wakabayashi, K., and Taguchi, R. (2011). Increase of oxidant-related triglycerides and phosphatidylcholines in serum and small intestinal mucosa during development of intestinal polyp formation in Min mice. Cancer Sci. *102*, 79–87.
17. Taguchi, R., Houjou, T., Nakanishi, H., Yamazaki, T., Ishida, M., Imagawa, M., and Shimizu, T. (2005). Focused lipidomics by tandem mass spectrometry. J. Chromatogr. B Analyt. Technol. Biomed. Life Sci. *823*, 26–36.
18. Wu, G., Sher, R.B., Cox, G.A., and Vance, D.E. (2009). Understanding the muscular dystrophy caused by deletion of choline kinase beta in mice. Biochim. Biophys. Acta *1791*, 347–356.
19. Miyagawa, T., Kawashima, M., Nishida, N., Ohashi, J., Kimura, R., Fujimoto, A., Shimada, M., Morishita, S., Shigeta, T., Lin, L., et al. (2008). Variant between CPT1B and CHKB associated with susceptibility to narcolepsy. Nat. Genet. *40*, 1324–1328.
20. Zweigner, J., Jackowski, S., Smith, S.H., Van Der Merwe, M., Weber, J.R., and Tuomanen, E.I. (2004). Bacterial inhibition of phosphatidylcholine synthesis triggers apoptosis in the brain. J. Exp. Med. *200*, 99–106.

Developmental Biology 361 (2012) 79–89

Contents lists available at SciVerse ScienceDirect

Developmental Biology

journal homepage: www.elsevier.com/developmentalbiology

Filamin C plays an essential role in the maintenance of the structural integrity of cardiac and skeletal muscles, revealed by the medaka mutant *zacro*

Misato Fujita [a,1,2], Hiroaki Mitsuhashi [b,1], Sumio Isogai [c], Takahiro Nakata [d], Atsushi Kawakami [a], Ikuya Nonaka [b], Satoru Noguchi [b], Yukiko K. Hayashi [b], Ichizo Nishino [b], Akira Kudo [a,*]

[a] Department of Biological Information, Tokyo Institute of Technology, 4259-B-33 Nagatsuta, Midori-ku, Yokohama 226-8501, Japan
[b] Department of Neuromuscular Research, National Institute of Neuroscience, National Center of Neurology and Psychiatry, 4-1-1 Ogawa-higashi, Kodaira, Tokyo 187-8502, Japan
[c] Department of Anatomy, School of Medicine, Iwate Medical University, 2-1-1 Nishitokuta, Yahaba, Shiwa 028-3694, Japan
[d] Department of Health Science, Ishikawa Prefectural Nursing University, 1-1 Gakuendai, Kahoku, Ishikawa 929-1210, Japan

ARTICLE INFO

Article history:
Received for publication 19 July 2011
Revised 5 October 2011
Accepted 6 October 2011
Available online 14 October 2011

Keywords:
Medaka mutant
Filamin C
Cardiac muscle
Skeletal muscle
zacro

ABSTRACT

Filamin C is an actin-crosslinking protein that is specifically expressed in cardiac and skeletal muscles. Although mutations in the filamin C gene cause human myopathy with cardiac involvement, the function of filamin C *in vivo* is not yet fully understood. Here we report a medaka mutant, *zacro* (*zac*), that displayed an enlarged heart, caused by rupture of the myocardiac wall, and progressive skeletal muscle degeneration in late embryonic stages. We identified *zac* to be a homozygous nonsense mutation in the *filamin C* (*flnc*) gene. The medaka filamin C protein was found to be localized at myotendinous junctions, sarcolemma, and Z-disks in skeletal muscle, and at intercalated disks in the heart. *zac* embryos showed prominent myofibrillar degeneration at myotendinous junctions, detachment of myofibrils from sarcolemma and intercalated disks, and focal Z-disk destruction. Importantly, the expression of γ-actin, which we observed to have a strong subcellular localization at myotendinous junctions, was specifically reduced in *zac* mutant myotomes. Inhibition of muscle contraction by anesthesia alleviated muscle degeneration in the *zac* mutant. These results suggest that filamin C plays an indispensable role in the maintenance of the structural integrity of cardiac and skeletal muscles for support against mechanical stress.

Introduction

Skeletal muscle and heart are the organs that produce physical force by muscle contraction, and muscle fibers are incessantly exposed to strong mechanical stress. To protect intracellular structures against such mechanical stress, muscle fibers express a variety of muscle-specific proteins that often form large complexes.

Two major protein complexes, the dystrophin-associated glycoprotein complex (DGC) and the integrin complex are known to have important roles in affording mechanical integrity to striated muscle. In skeletal muscle, these complexes, which are localized at the sarcolemma (Arahata et al., 1988; Mayer, 2003; Watkins et al., 1988) and myotendinous junctions (MTJs; (Bao et al., 1993; Samitt and Bonilla, 1990; Shimizu et al., 1989), where the muscle fibers are connected to tendon, link the subsarcolemmal actin cytoskeleton to the extracellular matrix (ECM) (Burkin and Kaufman, 1999; Campbell, 1995; Yoshida et al., 2000). Defects in the components of this DGC lead to muscular dystrophy (Bonnemann et al., 1995; Hoffman et al., 1987; Lim et al., 1995; Nigro et al., 1996; Noguchi et al., 1995; Roberds et al., 1994), an inherited muscular disorder characterized by progressive muscle degeneration, suggesting the importance of this linkage system for the integrity of muscle fibers. Muscle fibers specifically express α7β1 integrin, and a defect of α7 integrin causes muscular dystrophy, primarily affecting muscle fibers close to the MTJs (Hayashi et al., 1998; Mayer et al., 1997; Miosge et al., 1999), pointing to the importance of the integrin-based linkage for muscle integrity, particularly at MTJs. In heart, DGC and integrins are localized at the sarcolemma as well as at intercalated disks, which are the contact sites between cardiomyocytes (Anastasi et al., 2009; van der Flier et al., 1997).

The Z-disk is a huge multi-protein complex that constitutes the border of individual sarcomeres. This Z-disk plays a key role in the crosslinking of actin thin filaments of myofibrils to withstand the extreme mechanical force generated during muscle contraction. Z-disks are attached to the sarcolemmal DGC and integrin complexes at the sites of costameres via Z-disk-associated linker molecules (Ervasti, 2003). Recently, mutations in genes encoding Z-disk components have been found to be responsible for a group of muscle diseases termed myofibrillar myopathy, which is pathologically characterized by myofibrillar disorganization, including the degeneration of the

* Corresponding author. Fax: +81 45 924 5718.
E-mail address: akudo@bio.titech.ac.jp (A. Kudo).
[1] Misato Fujita and Hiroaki Mitsuhashi were equal contributors to this study.
[2] Present address. Section on Vertebrate Organogenesis, Program in Genomics of Differentiation, Eunice Kennedy Shriver National Institute of Child Health and Human Development, National Institutes of Health, MD 20892, USA.

0012-1606/$ – see front matter © 2011 Elsevier Inc. All rights reserved.
doi:10.1016/j.ydbio.2011.10.008

sarcomere structure (Selcen, 2008; Selcen et al., 2004). These reports suggest that Z-disk proteins have important roles in maintaining organized sarcomere structures.

Filamins are actin-crosslinking proteins first purified by their ability to bind and precipitate actin (Hartwig and Stossel, 1975; Stossel and Hartwig, 1975). Filamins are composed of 3 isoforms, filamins A, B, and C. All filamins consist of an N-terminal actin-binding domain followed by 24 immunoglobulin-like repeats, and they dimerize at the 24th repeat domain located at the C-terminus (Stossel et al., 2001). Filamins directly interact with more than 30 diverse proteins, and are involved in multiple cellular processes including cell–cell and cell–matrix adhesion, mechanoprotection, actin remodeling, and various intracellular signaling pathways (Feng and Walsh, 2004). Filamin C is a muscle-specific isoform and localizes at MTJs, costameres, Z-disks, and intercalated disks in mammal and avian muscles (Ohashi et al., 2005; van der Ven et al., 2000a). Interestingly, filamin C interacts with both DGC (Thompson et al., 2000) and integrin (Gontier et al., 2005; Loo et al., 1998), as well as with the Z-disk proteins myotilin (van der Ven et al., 2000b), FATZ-1 (Faulkner et al., 2000), and myopodin (Linnemann et al., 2010) through its C-terminal region. Such localization and protein interaction suggest that filamin C functions in maintaining the mechanical integrity of muscle cells. Recently, mutations in the filamin C gene were identified in patients having myofibrillar myopathy (Kley et al., 2007; Luan et al., 2010; Shatunov et al., 2009; Vorgerd et al., 2005). These patients frequently develop cardiac abnormalities in addition to skeletal myopathy, suggesting the essential role of filamin C in both skeletal and cardiac muscles. To investigate the function of filamin C *in vivo*, Dalkilic et al. (2006) generated *filamin C*-deficient mice having a deletion of the last 8 exons of *Flnc*. This deficient mouse shows fewer muscle fibers or primary myotubes than normal and abnormal rounded fibers, suggesting defects in primary myogenesis; however, this mouse does not present any cardiac defects, which indicates a partial-loss-of-function. Since these mice die *in utero* or live only a short while after birth, further detailed observations cannot be carried out.

Recently, zebrafish have emerged as an alternative model organism to study the vertebrate muscular system and to isolate new dystrophy-causing genes/pathways (Guyon et al., 2007; Steffen et al., 2007). A deficiency of DGC or integrin-linked kinase causes a muscular dystrophic phenotype in zebrafish embryos (Bassett et al., 2003; Cheng et al., 2006; Gupta et al., 2011; Guyon et al., 2005; Postel et al., 2008), suggesting that their functions are likely to be analogous to those in humans. In zebrafish embryos, the DGC is localized initially at the junctional area, where the ends of muscle fibers attach to the myosepta, corresponding to the myotendinous junction (MTJ). Loss of DGC causes muscle fiber detachment at MTJs, indicating compromised adhesion between muscle fibers and the ECM of myosepta. Medaka (*Oryzias latipes*), another teleost fish, has the experimental advantages of external development, transparency, and quick production of a number of embryos, similar to the zebrafish. Unlike zebrafish, however, various medaka inbred strains have been established; and the medaka genome, which is about one-half of the size of the zebrafish genome, is almost fully sequenced and aligned, indicating that the medaka has powerful advantages for the application of forward genetics (Ishikawa, 2000; Wittbrodt et al., 2002).

Here, we identified a medaka mutant, *zacro* (*zac*), that has a nonsense mutation, resulting in an early truncation at the 15th immunoglobulin-like repeat of the medaka orthologue of filamin C. This mutation causes myocardiac rupture in the ventricle. Although this mutant displayed normal myogenesis in myotome muscles during early stages of embryonic development, its myofibrils gradually degenerated and became disorganized in later stages. Detailed histological analysis suggests an indispensable role of filamin C in the maintenance of the muscle structure rather than in its formation in both heart and skeletal muscles.

Materials and methods

Medaka strains and mutant screening

All studies requiring wild-type medaka (*O. latipes*) were carried out by using the Qurt strain, which was derived from the southern population (Wada et al., 1998). Fish were maintained in an aquarium system with re-circulating water at 28.5 °C. Embryos were obtained from natural spawning, and incubated at 28 ± 2 °C. Stages were determined as previously described (Iwamatsu, 2004). *N*-ethyl-*N*-nitrosourea (ENU) was used for mutagenesis, and a standard genetic F3 screening for mutations affecting embryogenesis were performed as described earlier (Ishikawa, 1996; Ishikawa et al., 1999). The *zac* mutant was identified by microscopic inspection as a Mendelian-inherited recessive lethal mutation that caused a phenotype characterized by congestion in the blood vessels and pericardial edema.

Positional cloning

zac heterozygous fish, which were maintained on the southern Qurt genomic background, were mated with the northern HNI strain fish (Hyodo-Taguchi, 1980) to generate F1 families. Embryos for the genetic mapping were obtained from inter-crosses of F1 *zac* carriers. To locate the genetic linkage, we conducted bulk segregant analysis on pools of genomic DNA from *zac* mutants and wild-type embryos by using sequence tagged site (STS) markers on the medaka genome (Kimura et al., 2004). The *zac* region was narrowed down by using additional STS markers, AU171271 and Olb2110h (Naruse et al., 2000), and newly designed restriction fragment length polymorphism (RFLP) markers, HAL and KCND2 (HAL; 5′-GGATGGGCAGATGCCAAATATG-3′ and 5′-GTCCCGTTGATCAGAGCCAG-3′/MboI, KCND2; 5′-CAGCAGGTGTAGCGGCATG-3′ and 5′-GTTGGCCATCACTGATATGGC-3′/AfaI). cDNAs of *flnc* from *zac* mutant and wild-type embryos were amplified, and verified by sequencing. The full-length cDNA of *flnc* was cloned by PCR using primers including XbaI restriction enzyme sites [5′-CAATCTAGACAAGGAACAAGCC-3′ and 5′-GAATCTAGACCACCATTTAGCC-3′], and was sequenced. We obtained 2 different *flnc* clones, which appeared to be splice variants. To confirm the linkage between the *zac* mutation and *flnc* gene, we performed allele-specific PCR using 2 independent outer primers [5′-TTCAGTTGGAGGACATGGGAT-3′ and 5′-GACACCTGCAACACAACTCTA-3′] in combination with either a wild type-specific antisense primer [5′-CTTGCAGGTCACCTTTCCTTT-3′] or a mutant-specific one [5′-CTTGCAGGTCACCTTTCCTTA-3′]. We also performed 5′-RACE and 3′-RACE to obtain full-length sequence information on *flnc* cDNA. The sequences of the medaka *flnc* have been deposited in GenBank under the accession numbers AB639344 and AB639345.

Birefringence assay

Embryos were dechorionated at stage 27. Muscle birefringence was analyzed at stages 32 and 34 by placing anesthetized embryos on a glass dish and observing them with an underlit dissecting scope (Olympus, SZX12) having 2 polarizing filters (Olympus, SZX-P0 and SZX2-AN). The top polarizing filter was twisted until only the light refracting through the striated muscle was visible.

Histological analysis

Embryos were fixed overnight at 4 °C in 4% paraformaldehyde (PFA) in phosphate-buffered saline pH 7.4 (PBS), dehydrated by ethanol, and embedded in a resin (Technovit 8100, Kulzer Heraeus) according to the manufacturer's instructions. Sections were cut at 2 μm and stained with Harris's hematoxylin and Eosin Y or Masson trichrome staining buffer (SIGMA).

Whole-mount RNA in situ hybridization

Whole-mount RNA *in situ* hybridization was performed as previously described (Inohaya et al., 1995; Inohaya et al., 1999). Digoxigenin-labeled antisense RNA probes for cardiac myosin light chain 2 (*cmlc2*), desmin (*des*), *flnc*, *myf5*, *nkx2.5*, *tbx5a*, and ventricular myosin heavy chain (*vmhc*) were used. The primer sets used for cloning the respective probes are listed below.

cmlc2 F: AATGTCTTTTCCATGTTYGARC
R: CAGATTCAGCAGTTTAARGARG and CTCCTCTTTCTCATCHCCATG
des F: AACAACCAGCCAACCATGAGC
R: ACAGATGTAGTTATCCTGCAGG
flnc F: GCTCCAGAGGAAATTGTGGAC
R: CTCACACCTTTAGGCTGTAGC
myf5 F: ATCCACTTCTTCTCCCCAGC
R: TTTCTCCTCAGAGAGAACCG
*nkx2.5*F: TTCTCTCAGGCGCAGGTGTACGAGC
R: GCDGGGTAGGYGTTGTA
tbx5a F: GTCTGAGATTTTCCGAGCTCC
R: CTCTCTCTAGACTCGAGTTGGTCCTTCTTGTGTTCTCCC
vmhc F: GGAGCTGGATGATGTGGTTTC
R: CATGGGCTAAGGCGTTCTTGGC
(R: A,G. Y: C,T. H: A,C,T)

Injection of morpholino antisense oligonucleotide (MO)

We obtained a specific MO (Gene Tools) to interfere with *flnc* translation. The MO [5′-GGCCATCATGTTGGCTTGTTCCTTG-3′] was dissolved at concentrations from 100 to 1000 μM in nuclease-free water. Approximately 0.5 nl of MO solution or standard control MO [5′-CCTCTTACCTCAGTTACAATTTATA-3′] was injected into 1-cell-stage embryos.

Whole-mount immunofluorescence

Dechorionated embryos were anesthetized in 0.02% tricaine methanesulfonate and fixed in 4% PFA in PBS at 4 °C overnight. We used chilled methanol at −20 °C as the fixative for anti-laminin antibody, and IHC Zinc fixative (BD Biosciences) for anti-γ-actin antibody. After fixation, embryos were dehydrated in a graded series of methanols (25–50–75%) and stored in 100% methanol at −20 °C. Embryos were rehydrated in a graded series of methanols (75–50–25%) and washed 3 times for 15 min each time in MABTr (0.1 M maleic acid and 150 mM NaCl containing 0.1% Triton X-100) and subsequently in MABDTr (MABTr with 1% BSA and 1% DMSO) twice for 30 min each time. Following blocking with 5% goat serum in MABDTr for 30 min, the embryos were incubated with primary antibodies at 4 °C overnight. The following antibodies were used: anti-filamin C (SIGMA HPA006135; 1:100), anti-vinculin (SIGMA V4505; 1:50), anti-α-actinin (SIGMA A7811; 1:500), anti-integrin β1D (Millipore MAB1900; 1:25), anti-β-sarcoglycan (Novocastra NCL-b-SARC; 1:50), anti-slow muscle myosin heavy chain (F59, DSHB; 1:100), anti-FAK pY397 (Invitrogen 44-625G; 1:100), anti-dystrophin (SIGMA D8043; 1:100), anti-β-dystroglycan (Novocastra NCL-b-DG; 1:100), and anti-phospho-paxillin (Cell Signaling Technology #2541; 1:50). Rabbit polyclonal anti-cytoplasmic γ-actin antibody was previously characterized (Nakata et al., 2001), and used at a dilution of 1:100. Embryos were washed 6 times in MABDTr for 15 min each time, and then incubated with Alexa488-conjugated anti-rabbit IgG or Alexa568-conjugated anti-mouse IgG (Molecular Probe; 1:800) at 4 °C overnight. Primary and secondary antibodies were diluted in Can Get Signal immunostain solution A (TOYOBO). After 6 more washings in MABTr, the embryos were whole-mounted on glass slides and observed with a confocal microscope (LSM 700, Zeiss).

Electron microscopy

For observation using transmission electron microscope (TEM), embryos were dechorionated and fixed at stage 27, 29, 30, 32 or 36 in 100 mM cacodylate buffer (pH 7.4) containing 2% glutaraldehyde and 4% PFA at 4 °C overnight. Samples were post-fixed in 0.06 M s-collidine buffer (pH 7.2) containing 1.3% osmium tetroxide and 0.5% lanthanum nitrate, dehydrated by passage through a graded series of ethanols, and finally embedded in Epon 812 (Taab). Longitudinal sections (120 nm) were stained with 3% uranyl acetate for 20 min and then with 0.4% lead citrate for 5 min. Sections were viewed with a Tecnai Spirit transmission electron microscope (FEI) or a Hitachi H-7100 or H-7650 electron microscope (Hitachi).

For observation using scanning electron microscopy (SEM), embryos were fixed in 0.1 M phosphate buffer (PB, pH 7.4) containing 2.5% glutaraldehyde and 2% PFA. The yolk were removed from the embryo with forceps to expose the heart, and postfixed for 2 h in 1% osmium tetroxide in PB at 4 °C. The embryos were then rinsed in PB, dehydrated in a graded series of ethanol, frozen in t-butyl alcohol, then freeze-dried *in vacuo* with an Eiko ID-2. The embryos were mounted on a metal stub, osmium-coated by using a Filgen OPC60A, and observed with an HS-6 electron microscope (Hitachi).

Muscle relaxation assay

Embryos were incubated with anesthetized in 0.0015% tricaine methanesulfonate in embryo medium for 48 h from stages 27 to 32 to prevent muscle contractions. Treated and untreated embryos were immunostained with F59 antibody obtained from the Developmental Studies Hybridoma Bank at stage 32, and the number of somites with muscle-fiber degeneration was counted.

Results

Enlarged ventricle and muscle disorganization in zac mutants

zacro (*zac*) is a recessive, embryonic-lethal mutant obtained by ENU (*N*-ethyl-*N*-nitrosourea) mutagenesis. *zac* mutants were characterized by an abnormally enlarged heart with a gradually reduced blood flow. The normal medaka heart starts to beat at stage 24, and blood flow begins at stage 25. No difference was observed until stage 25 in *zac* embryos; however, by stage 28 prior to the heart looping, *zac* mutants showed blood congestion in the ventricle along with pericardial edema (Figs. 1A, B). Ruptures in the myocardium layer were detected in the *zac* mutants at stage 27, especially in the dorsal-right myocardium of the ventricle (Figs. 1C, D asterisk). As the endocardium was intact in *zac* mutants, we speculate that the blood accumulation was caused by ineffective contraction of the torn myocardium. *zac* mutants appeared to be normal in their somite differentiation during the early stages of somitogenesis; however, by stage 32, they frequently exhibited an abnormal curvature with their tails dorsally up instead of having the normal flat body axis (Figs. 1E, F). We further analyzed the birefringence of myotome muscle of *zac* mutants by using polarized filter microscopy. Birefringency is used to assess muscle organization in zebrafish models of muscle disease (Granato et al., 1996). Wild-type embryos from stage 32 onwards displayed high birefringence due to the ordered array of their myofilaments (Figs. 1G, I), whereas *zac* mutants displayed patchy birefringence at this stage (Fig. 1H), indicating muscle disorganization in some somites. Muscle disorganization in the *zac* mutant continued to progress, and most of the somites lost their birefringence by stage 34 (Fig. 1J). Histological analysis revealed that orientation of each myotube was severely disorganized by stage 40 (Figs. 1K, L).

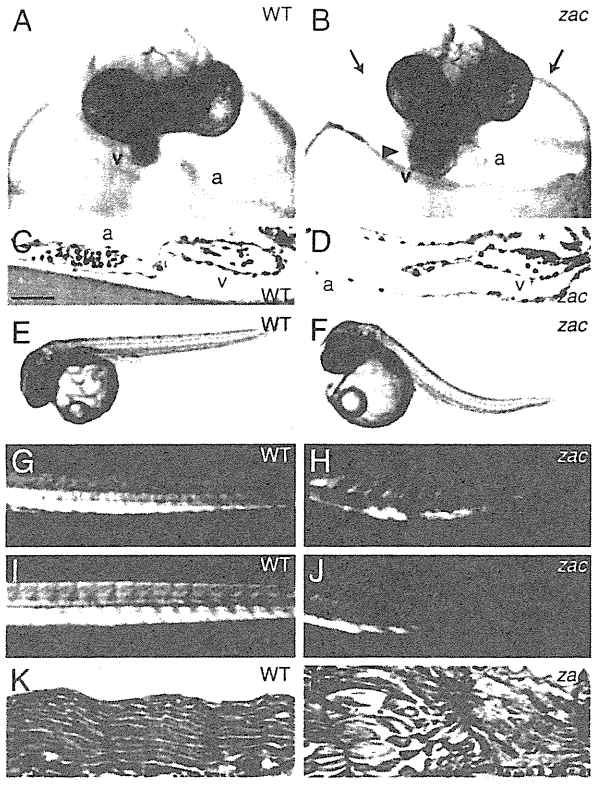

Fig. 1. Cardiac and skeletal muscle phenotypes of *zac* mutants. Embryos from the wild-type (A, C, E, G, I, K) and *zac* mutants (B, D, F, H, J, L). (A, B) Ventricular enlargement in *zac* mutants. Frontal views at stage 28. Dorsal is to the top. Blood cell accumulation in the ventricle (B, arrowhead) and cardiac edema (B, arrows) are visible. a; atrium, v; ventricle (C, D) Hematoxylin and eosin staining of a sagittal section of heart at stage 27. Rostral is to the left. Only the myocardial wall has a rupture (D, asterisk). Scale bar: 20 μm in "C." (E, F) Whole view from the lateral side at stage 32. *zac* mutants show body curvature. (G–J) Birefringence of skeletal muscle at stage 32 (G, H) and stage 34 (I, J). Rostral is to the left. *zac* mutant shows patchy birefringence at stage 32 and overall reduction in birefringence at stage 34. (K, L) Masson trichrome staining of horizontal sections at stage 32. Rostral is to the right. Striated patterns of sarcomeres can be seen in many muscle cells, but some myofibers have severely degenerated in the *zac* mutants. Scale bar in "K": 20 μm.

After hatching, *zac* mutants were not able to swim normally, and they died around 14 days post-fertilization. These phenotypes indicate that the *zac* mutation affected both cardiac and skeletal muscles.

Nonsense mutation in flnc in zac mutants

We performed positional cloning to identify the responsible gene in *zac* mutants. By using sequence-tagged site (STS) markers (Kimura et al., 2004), we mapped the *zac* gene to the marker MF01SSA047D04 on the medaka linkage group 6 (Fig. 2A). We searched the expressed sequence tag (EST) markers around the MF01SSA047D04, and found zero and 2 independent recombinants by using AU171271 and Olb2110h, respectively. Therefore, the *zac* gene was placed in the vicinity of AU171271 between MF01SSA047D04 and Olb2110h (Fig. 2A). We further performed fine mapping by utilizing an additional marker, histidine ammonia-lyase (*HAL*), which gave 1 recombinant and narrowed down the *zac* locus. We also found zero recombinants by using another marker, the potassium voltage-gated channel, Shal-related subfamily, member 2 (*KCND2*). Though the genomic sequence encompassing the *zac* locus contained several open reading frames (ORFs), one of them encoded a protein highly homologous to human filamin C, a cardiac and skeletal muscle-specific isoform of the filamin family.

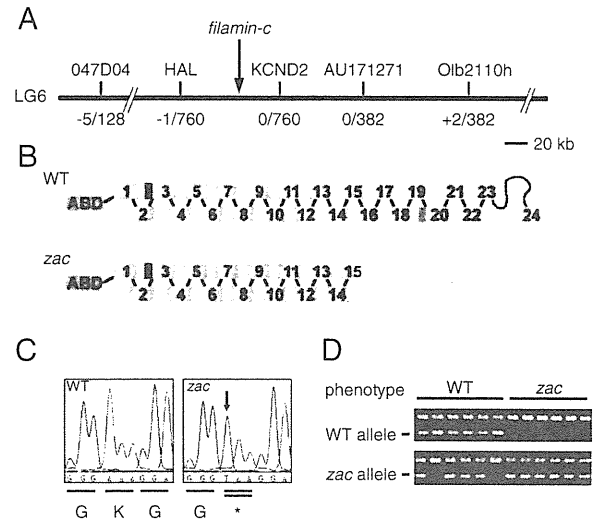

Fig. 2. Positional cloning of *zac* gene (A) Map of the genomic region containing the *zac* gene. The *zac* locus is mapped on the medaka linkage group (LG) 6 by using M-markers, and *flnc* is located in the candidate region. HAL, histidine ammonia-lyase and KCND2, potassium voltage-gated channel, Shal-related subfamily, member 2. Recombination frequencies for the respective markers are shown below. (B) Schematic drawings of filamin C protein in wild-type and *zac* mutant. The actin-binding domain (ABD) is located at N-terminal followed by 24 repeats of filamin domains. The red region between the 2nd and 3rd repeats indicates the unique splicing variation in medaka fish. The green box between the repeats 19th and 20th is a unique sequence in filamin C members. There is only one hinge sequence between the repeat 23rd and 24th in the medaka filamin C. (C) Chromatogram of the cDNA sequence containing a nonsense mutation from A to T in a coding region of *flnc* (arrow). (D) Linkage of *zac* mutation with *flnc* as shown by allele-specific genotyping PCR. WT indicates phenotypically wild-type embryos, so some are genotypically heterozygotes revealing both WT and zac alleles' PCR products and others are genotypically wild-type having WT allele's PCR product only. All *zac* mutants are genotypically homozygotes, which show the zac allele's PCR products only.

The sequence analysis revealed that the medaka *flnc* had a high degree of homology (approximately 77% amino acid identity) to the human *FLNC* (Supplementary Fig. 1). The overall structure of medaka filamin C consisted of the actin-binding domain (ABD) and 24 immunoglobulin-like repeats with a hinge region between the 23rd and the 24th repeats (Fig. 2B). Although there was no spacer region between the 15th and the 16th repeats, as found in chicken *Flnc/cgABP260* (Ohashi et al., 2005) and in some human *FLNCs* (Supplementary Fig. 1), the medaka *flnc* had a C-isotype-specific insertion sequence between the 19th and the 20th repeats (green box in Fig. 2B; blue underline in Supplementary Fig. 1), which is also seen in mouse *Flnc* (Dalkilic et al., 2006). We also found a novel splicing variation of an additional 39 amino acids between the 2nd and 3rd repeats (red box in Fig. 2B).

We sequenced the entire coding sequence of medaka *flnc* from the *zac* mutant and the wild-type sibling alleles and found that the *zac* mutant had a nucleotide substitution from A to T at the first base of codon 1680 (Fig. 2C; AAA to TAA). As a result, this mutation changed the lysine residue to a stop codon (K1680X), causing premature termination in the 15th immunoglobulin-like repeat. This mutation was detected with 100% identity by PCR using allele-specific primers (Fig. 2D).

In the medaka genome database from Ensembl, there is one more filamin C ortholog, which is notated as FLNC (2 of 2). This predicted gene is located mostly in the ultracontig278 and partially in the scaffold698_contig104802. To find the possibility of functional contribution, we examined the sequence similarity of this gene compared to the human filamin C and the medaka filamin C investigated in this study (Supplementary Fig. 2). FLNC (2 of 2) is described as "ol filamin c #3" in this figure. The FLNC (2 of 2) contains 16 filamin-repeats from 9th to 24th repeat of the regular filamin C, and has one hinge region between 23rd and 24th repeat. About three fourth of filamin C-specific region (UR) is pulled out and N-terminal domains of the

actin binding domain and 1–8th repeats are missing. Although the entire sequence is well conserved and the feature of having single hinge represents filamin C, the lack of N-terminal domains is critical. This gene might be termed as "ol flnc 9–24" (Stossel et al., 2001) and functional redundancy would not be expected as for filamin C.

mRNA expression of flnc is markedly reduced in zac mutants

The pattern of *flnc* expression was analyzed by whole-mount RNA *in situ* hybridization. *flnc* expression was first evident in somites and at the rostral tip of notochord at the onset of somitogenesis. Subsequently, by the 6-somite stage, the expression of *flnc* was detected in the cardiac precursor cells in the anterior lateral-plate mesoderm (Fig. 3A). After migration of the myocardial precursor cells towards the midline, the expression of *flnc* was detected in both the atrium and ventricle (Fig. 3C). These expressions of *flnc* in the somites, the rostral tip of the notochord, and the cardiac muscles continued in subsequent stages (Fig. 3E). At later stages, additional expression was seen in the muscles of the pectoral fin joint and head (data not shown). Although the pattern of expression of *flnc* did not differ between the wild-type and *zac* mutants, the level of expression was reduced in the latter (Figs. 3B, D, F).

To further identify whether this lower expression of *flnc* in *zac* mutants was caused by the transcriptional down-regulation or not, we generated a transgenic medaka line expressing EGFP under the regulation of a 3 kb-*flnc* promoter. Both in the wild-type and *zac* mutants, the EGFP transgene was expressed at a similar level (Figs. 3G, H), demonstrating that the transcription of the *flnc* gene was not affected by the *zac* mutation. Moreover, the reduced mRNA expression of *flnc* in *zac* mutants was detected before the appearance of abnormal cardiac and muscular phenotypes (Figs. 3A, B), suggesting that the reduction was not caused by any morphological effect in the *zac* mutants. Taken together, these results suggest that the apparently lower expression of *flnc* in *zac* mutants may have been due to the instability of the mutated mRNAs, as often observed in other cases (Baker and Parker, 2004).

To confirm whether the defect in *flnc* was sufficient to cause the *zac* phenotype, we used morpholino antisense oligonucleotides (MO) targeting the translation of *flnc*. When the MO was injected at a dose of 400 μM, 13% of the injected embryos displayed a *zac*-like cardiac phenotype including the myocardial ruptures (n = 94; Figs. 3I, J). In contrast to the heart phenotype, we did not observe an abnormal phenotype in the skeletal muscles of the MO-injected embryos. It appears that the MO may have required a longer time before producing the skeletal muscle phenotype, but the effect of MO might not have been strong enough to affect the skeletal muscles. We tested higher concentrations of MO (500–1000 μM); however, the overall shape of the injected embryos was severely deformed.

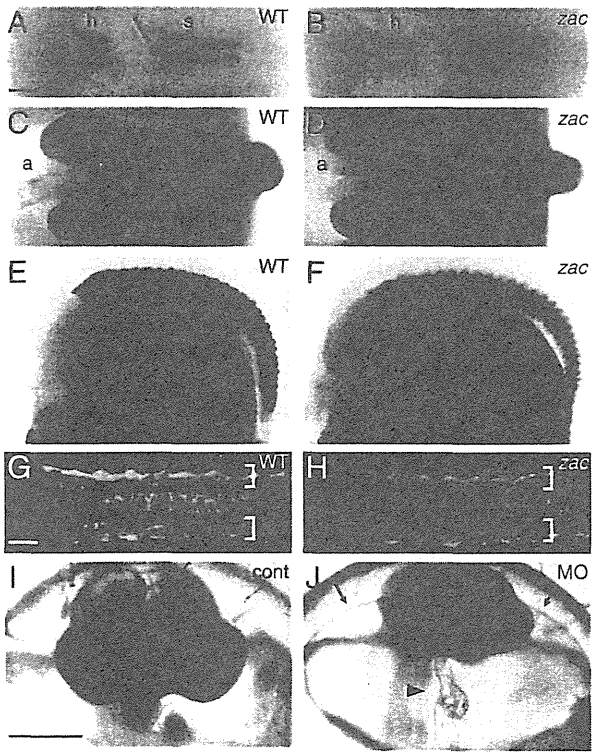

Fig. 3. Expressions of medaka *flnc* in notochord and cardiac and skeletal muscles. Wild-type (A, C, E, G) and *zac* mutant embryos (B, D, F, H). (A–F) Whole-mount RNA *in situ* hybridization analysis of *flnc* expression at stage 22 (A, B) and stage 27 (C–F). Dorsal views (A–D) and lateral views (E, F). Rostral is to the left. *flnc* expression is seen in bilateral cardiac precursor cells (h), somites (s), and the anterior tip of the notochord (arrow). Both atrium (a) and ventricle (v) express *flnc*. Note that *flnc* mRNA expression is reduced in *zac* embryos (B, D, F). (G, H) *flnc* expression visualized in the *flnc* promoter transgenic medaka at stage 26. Dorsal views of the trunk. Rostral is to the left. The level of EGFP expression is not decreased in *zac* mutants, demonstrating that the decrease in the *flnc* mRNAs may be due to instability of mutated *flnc* mRNAs. Yellow and red brackets indicate somites and notochord, respectively. (I, J) Phenocopy by injection of MO. Stage 28. Head frontal views. Dorsal is to the top. Embryos injected with the control MO show the normal appearance (I). However, embryos injected with *flnc*-MO show the cardiac rupture in the ventricle (J: arrowhead) and edema (J: arrows). Scale bars: 100 μm in "A", 50 μm in "G" and 200 μm in "I".

zac mutation affects the maintenance of the muscle structure rather than its formation

Since the expression of *flnc* in medaka embryos was detected in the early stage of development (see Fig. 3), we investigated whether the *zac* mutation affected the differentiation of cardiac or skeletal muscle cells by examining the expression of various differentiation marker genes. The expression patterns and levels of cardiac differentiation markers, such as *nkx 2.5*, *tbx5a*, *des*, *cmlc2*, and *vmhc*, were not changed in *zac* hearts at stage 27 (Figs. 4A, B: *cmlc2*, C, D: *des*, the data for *nkx 2.5*, *tbx5a*, and *vmhc* are not shown). The expressions of muscle differentiation markers such as *myoD*, *myf5*, and *des* were also normal in the trunk and tail up to stage 30 (Figs. 4E–H). These results suggest that the early differentiation of cardiac and skeletal muscle cells was not affected in the *zac* mutants.

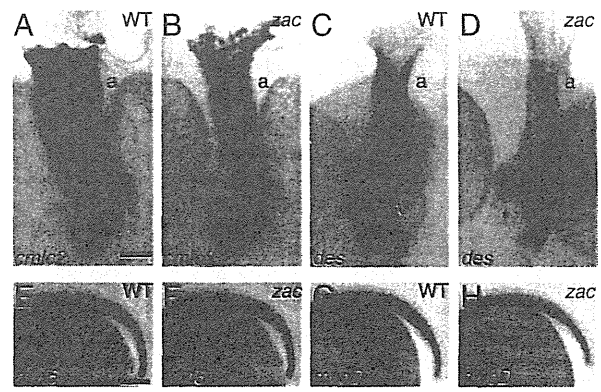

Fig. 4. Expressions of differentiation marker genes in cardiac and skeletal muscle development (A–D). Whole-mount RNA *in situ* hybridization for the expression of cardiomyocyte markers, *i.e.*, *cmlc2* (A, B) and *des* (C, D) at stage 27. Wild-type (A, C) and *zac* mutants (B, D). Dorsal view (A, B) and ventral view (C, D) are shown. Rostral is to the top. Differentiation of cardiomyocytes looks normal. A rupture of the myocardium in the *zac* ventricle is indicated by the asterisk. a; atrium and v; ventricle (E–H) Whole-mount RNA *in situ* hybridization for the expression of muscle markers *myf5* (E, F) and *myoD* (G, H) at stage 27. Wild-type (E, G) and *zac* mutants (F, H). Lateral views. Head is to the left. Both genes show normal expression patterns in the *zac* mutant. Scale bars: 20 μm in "A" and 200 μm in "E".

It has been demonstrated that filamin C protein is localized at the myotendinous junction, Z-disks, and sarcolemma in skeletal muscle fibers, and in the intercalated disks of cardiomyocytes in mammalian and avian hearts (Ohashi et al., 2005; Thompson et al., 2000; van der Ven et al., 2000a). To determine the subcellular localization of filamin C protein in medaka, we performed immunostaining with a filamin C-specific antibody. In the medaka heart, filamin C was localized at cell–cell contact sites between the cardiomyocytes (Fig. 5A). In skeletal muscle, the most abundant expression of filamin C was detected at the junction area where the ends of the muscle fibers attached to the myosepta (Fig. 5B), corresponding to the myotendinous junction (MTJ) in mammals (Summers and Koob, 2002). Filamin C was also localized at the sarcolemma (Figs. 5C–E) and Z-disks (Figs. 5F–H). These results suggest that the localization of filamin C protein is conserved among fish, avians, and mammals.

To examine the effect of filamin C-deficiency on muscle cells, we analyzed *zac* mutants by using a scanning electron microscope (SEM). At stage 27, cardiomyocytes in the *zac* mutant ventricle were not well-ordered ones and had a rougher surface with a number of lamellipodia- and filopodia-like structures (Figs. 6B, D) compared with those in the wild-type heart (Figs. 6A, C), although there was no significant difference in the atrium. These changes were more evident after the onset of blood circulation. Transmission electron microscopic (TEM) analysis of the wild-type heart revealed that organized myofibrils ran along the inner surface side of the cardiomyocytes with the nuclei being located at the outer surface side (Fig. 6E). In contrast, the cytoplasmic structure and subcellular localization of nuclei were severely disorganized in the *zac* mutant (Fig. 6F). Although myofibrils were present even after the rupture of the heart, which is consistent with the fact that the *zac* heart was able to contract, it is also important to note that fewer sarcomere bundles were attached to the intercalated disks in the *zac* mutants (Figs. 6G, H). Large vacuoles, which contained no sarcoplasmic or membranous materials, were observed in *zac* cardiomyocytes (Fig. 6H). The muscle sarcomere is the important structure for establishing cell–cell adhesion at the intercalated disk between the myocardial cells. Our observations suggest that the *zac* mutation may have interfered with the formation and/or maintenance of the sarcomere structures in the myocardium and that weakened cell–cell adhesion might have resulted in the rupture frequently seen in the ventricle, which is supposed to resist high contraction pressure.

Skeletal muscle was also analyzed by TEM. Although *flnc* was expressed from the onset of somitogenesis, the sarcomere structures in the *zac* mutants were normally formed in most of the skeletal muscle fibers and maintained even at stage 30 (Figs. 7A, B). Only in some somites of *zac* mutants had myofibrils degenerated at MTJs at stage 32 (Figs. 7C–F). In addition, focal disorganization of the sarcomere structure was observed in *zac* mutants. In the disorganized area, Z-disks were faint or totally missing (Figs. 7G, H). Many large vacuoles were also observed in *zac* skeletal muscle (Figs. 7I, J). The sarcolemma was frequently detached from the myofibrils, and dilated sarcoplasmic reticula occupied the space between them, in

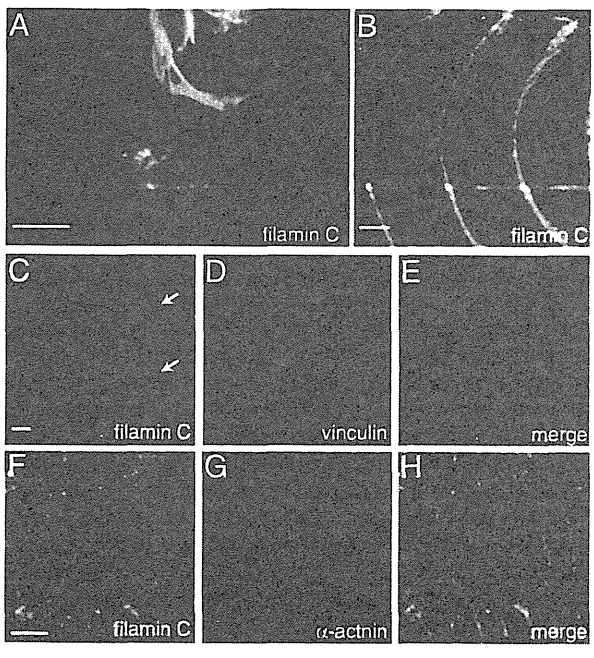

Fig. 5. Subcellular localization of filamin C protein in heart and skeletal muscles. Immunofluorescence staining of filamin C protein in the wild-type embryos. Filamin C is localized at cell–cell contact sites in the heart at stage 32 (A), in the junctional area where the ends of muscle fibers attach to the myosepta (corresponding to myotendinous junction) at stage 32 (B), and in the sarcolemma (C, arrows and merge in "E"), and Z-disks (F and merge in "H") at stage 40. (C–E) Double staining of filamin C (C), vinculin (D), and their merged image (E). (F–H) Double staining of filamin C (F), α-actinin (G), and their merged image (H). (B–H) Rostral is to the left. Lateral view. Scale bar: 20 μm in "A" and "B", 2 μm in "C" and 4 μm in "F".

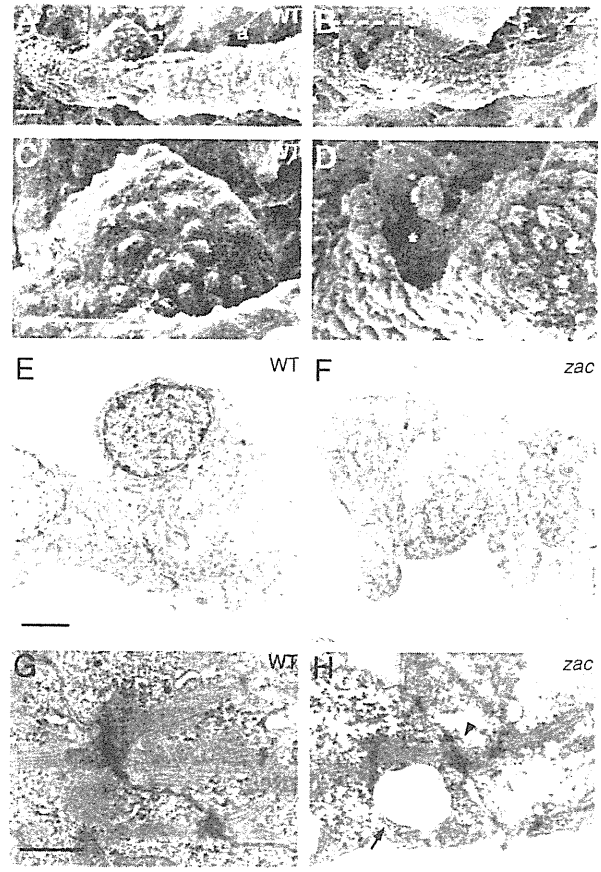

Fig. 6. Ultrastructure of cardiomyocytes. Embryos from the wild-type (A, C, E, G) and *zac* mutants (B, D, F, H). (A–D) Scanning electron microscopic analysis of heart tube at stage 27. Ventral views. Rostral is to the right. "C" and "D" are high magnifications of the boxed area in "A" and "B", respectively. Cardiomyocytes around the rupture (asterisk) in the *zac* heart show a rough and irregular cell surface. a; atrium and v; ventricle. (E–H) Transmission electron microscopic analysis of cardiomyocytes at stage 27. (E, F) Outer surface of the heart tube is to the top. Cardiomyocytes in *zac* mutants show an abnormal subcellular organization. (G, H) Ultrastructure of intercalated disks at stage 29. Fewer sarcomere bundles are connected to the intercalated disks in *zac* mutants (H, arrowhead) compared with their number in the wild-type (G) at stage 29. Large vacuoles are frequently observed in the *zac* mutants (H, arrow). Scale bar: 20 μm in "A", 10 μm in "C", 2 μm in "E" and 1 μm in "G".

the *zac* muscle at stage 36 (Figs. 7K, L). These results suggest that filamin C may have contributed to the stabilization of myofibrils at the MTJ, maintenance of the Z-disk structures, and attachment of myofibrils to sarcolemma rather than be involved in myofibril formation.

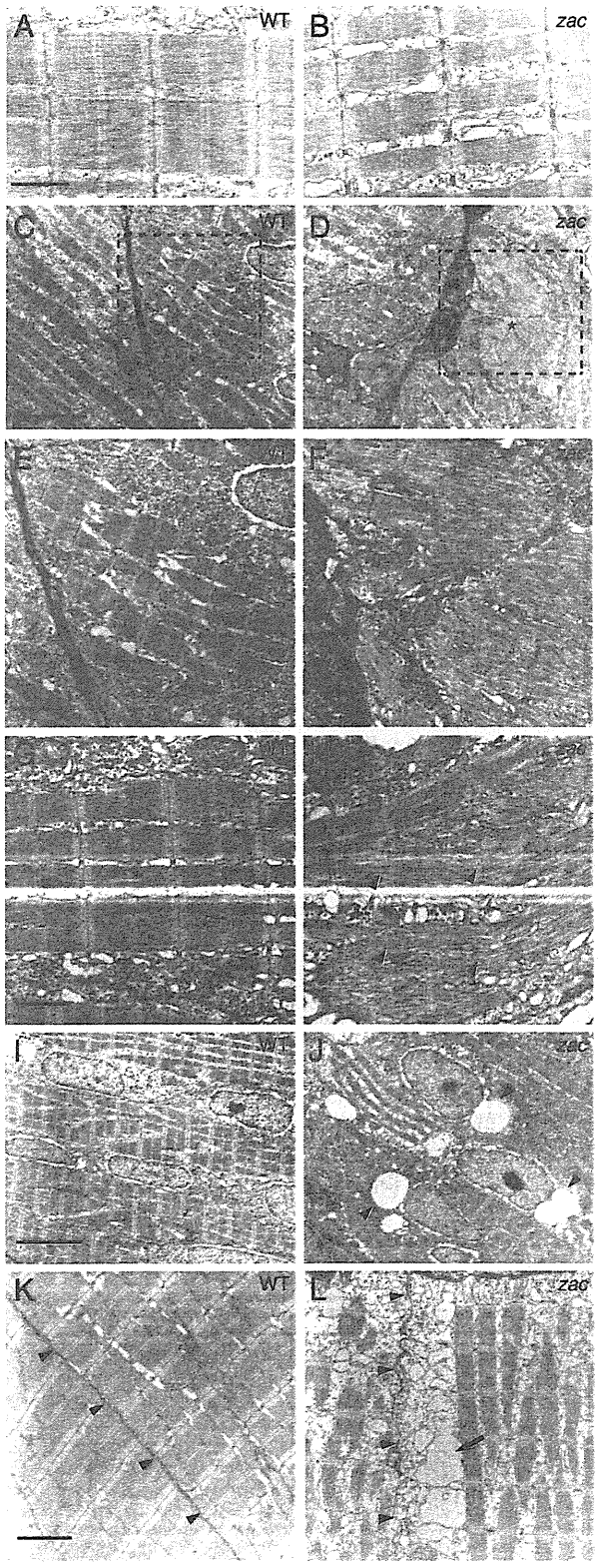

Reduction in amount of γ-actin at MTJs

Filamins crosslink actin filaments, and link them to cellular membrane by binding to the transmembrane proteins (Stossel et al., 2001). Filamin C interacts with β1-integrin (Gontier et al., 2005; Loo et al., 1998) and δ/γ-sarcoglycans (Thompson et al., 2000), the components of the DGC. Both complexes are concentrated at MTJs, and have an important role to link subsarcolemmal γ-actin filaments to the ECM in mammals. Since muscle fibers at the MTJs were affected in *zac* mutants, we evaluated the effect of the *zac* mutation on the localization of the proteins involved in this linkage system. Since we did not find any antibodies crossreactive with medaka δ/γ-sarcoglycans, we assessed the sarcoglycan complex by using antibodies against β-sarcoglycan (β-SG). It is known that the entire sarcoglycan complex, containing α-, β-, γ-, and δ-sarcoglycans, becomes destabilized, resulting in decreased localization at the sarcolemma, when any one of its components is disrupted in mammals or zebrafish (Guyon et al., 2005; Mizuno et al., 1994). Similar to the filamin C, integrin β1D, β-sarcoglycan (β-SG), and γ-actin were accumulated at the MTJ in the wild-type medaka (Fig. 8, upper panels). Although the expressions of integrin β1D and β-sarcoglycan were not altered in the *zac* mutants, γ-actin was markedly reduced at their MTJs (Fig. 8, lower panels). We also analyzed β-dystroglycan and dystrophin (other components of the DGC) and the phosphorylated forms of FAK and paxillin (downstream molecules of integrin signaling). The results revealed that these molecules were also accumulated at MTJs with no obvious difference in signals between the wild-type and *zac* mutants (data not shown). Since the filamin C is also localized at Z-disks (see Figs. 5F–H), we examined whether the filamin C mutation primarily affected the formation of Z-disks. Double immunostaining of γ-actin and α-actinin revealed that at stage 32 when γ-actin was already altered (Supplementary Fig. 3, upper panels), α-actinin-stained Z-disks were detected normally in *zac* myotome muscle (Supplementary Fig. 3, lower panels), indicating that the primary consequence of the deficiency of filamin C is the defect in the linkage system, not in the Z-disk. These results suggest that filamin C functions to maintain the structural integrity at the MTJs via γ-actin.

zac mutant is more susceptible to mechanical stress by muscle contraction

The observations by electron microscopy and immunohistochemistry demonstrated that muscle degeneration occurred not equally but stochastically in the *zac* mutants. In addition, muscle damage was frequently observed at MTJs, where myofibrils are exposed to strong mechanical stress from muscle contraction. These observations led us to investigate whether muscle degeneration was related to muscle contraction. So we incubated medaka embryos in a solution of tricaine methanesulfonate, which is a common reagent for anesthetizing fish by blocking the action potential. We found that a 0.0015% solution of tricaine methanesulfonate could suppress muscle contraction in medaka embryos without blocking heart beats at stage 27. Under this condition, all embryos survived from stages 27 to 32. So we incubated embryos in this anesthetic and evaluated muscle

Fig. 7. Ultrastructure of longitudinal section of skeletal muscle. Embryos of wild-type (A, C, E, G, I, K) and *zac* mutant (B, D, F, H, J, L). (A, B) Sarcomere structures are normally formed in *zac* mutants at stage 30. (C–F) Myofibrils have degenerated at myotendinous junctions (asterisk) at stage 32. "E" and "F" are high magnifications of the boxed area in "C" and "D", respectively. (G, H) Focal disorganization of the sarcomere structure at stage 32. Z-disks are not observed in some myofibrils in *zac* mutants (H, arrowheads). (I, J) Large vacuoles (J, arrowheads) are frequently observed in *zac* mutants at stage 32. They are single-membrane vacuoles, and no sarcomeric or membranous material is seen inside. (K, L) Detachment of sarcolemma from myofibrils in *zac* mutants at stage 36. Even though sarcomere structures are well-preserved, the sarcolemma (arrowheads) has become detached, and dilated sarcoplasmic reticula (L, arrow) occupy the space in *zac* mutants. Scale bar: 1 μm in "A" and "G", 5 μm in "C" and "I" and 2 μm in "E" and "K".

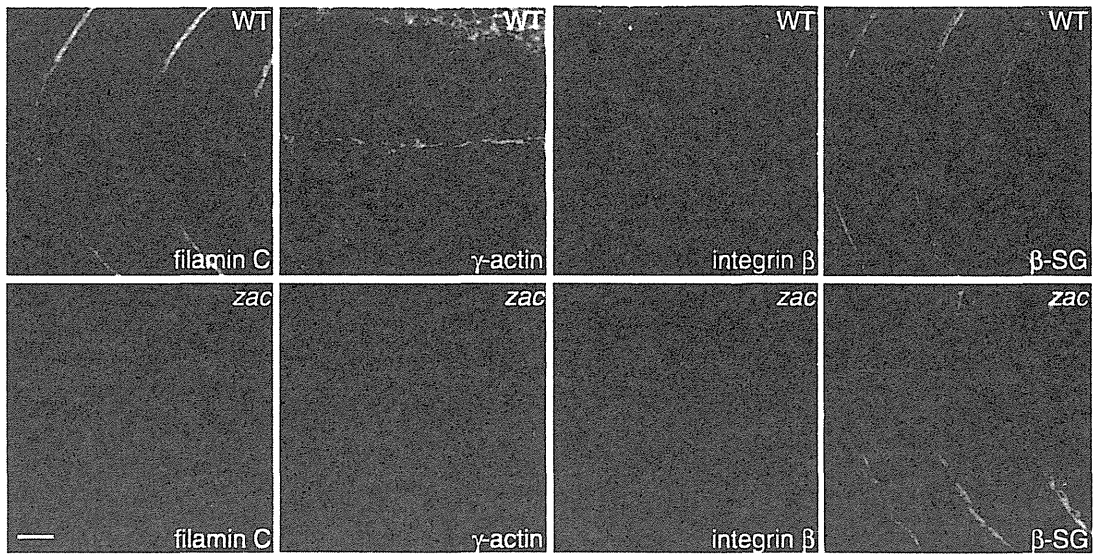

Fig. 8. Immunofluorescence analysis of MTJ. Immunofluorescence stainings of filamin C, γ-actin, integrin β1D and β-sarcoglycan (β-SG). Each of these proteins accumulates prominently at the MTJ in the wild-type. Only γ-actin protein expression is reduced in the *zac* mutants, whereas other proteins are retained. Rostral is to the left. Stage 32. Scale bar: 20 μm.

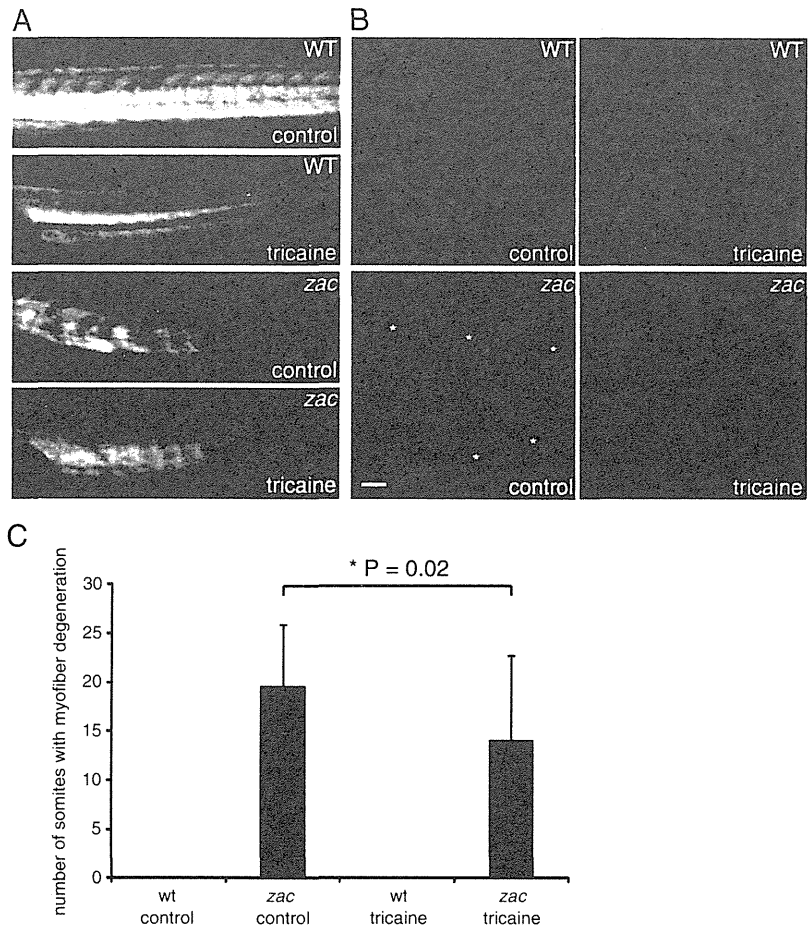

Fig. 9. *zac* mutant is more susceptible to mechanical stress by muscle contraction. (A) Birefringence assay of embryos in the control medium or in the medium containing the anesthetic tricaine methanesulfonate (tricaine). The anesthetized *zac* mutant shows a milder reduction in muscle birefringence compared with the non-treated *zac* mutant. (B) Slow muscle myosin heavy chain staining (F59) of control and anesthetized fish at stage 32. Asterisks show somites having muscle fiber degeneration. Scale bar: 20 μm. (C) Quantification of muscle degeneration. N = 20, P = 0.02.

degeneration. Anesthetized wild-type embryos appeared to be a bit smaller and skinnier compared with non-treated wild-type embryos, but did not show any perturbed birefringence. As expected, inhibition of locomotion restored muscle birefringence in the *zac* mutants (Fig. 9A). This finding was further confirmed by immunostaining of the slow muscle myosin heavy chain, which staining revealed a decreased level of myofiber disorganization in the anesthetized *zac* mutants (Figs. 9B, C). The myofibers in anesthetized wild-type embryos were thinner than those in the non-treated wild-type embryos, but never had degenerated or become disorganized. Loss of accumulation of γ-actin at the MTJs was not recovered under the tricaine treated condition in the *zac* mutants (data not shown), suggesting that the defect of γ-actin is not contraction-dependent. This is rather supporting the idea that γ-actin is linked to the MTJs by filamin C to reinforce the muscle structure. These results suggest the protective role of filamin C against the mechanical stress to myofibrils caused by muscle contraction.

Discussion

Function of filamin C in the heart

Mutations in human *FLNC* cause a myopathy with altered myofibril organization (Kley et al., 2007; Luan et al., 2010; Shatunov et al., 2009; Vorgerd et al., 2005). These patients frequently show a cardiomyopathy, but the mechanisms causing the cardiac symptom elicited by the each mutation in filamin C have remained unclear. We found that the loss of filamin C in medaka led to cardiac rupture in the ventricular myocardium. Unlike other fish mutants of muscle sarcomere proteins, for example, *pik/ttna* and *sih/tnnt2* (Sehnert et al., 2002; Xu et al., 2002), in which heart beating is severely damaged, the *zac* mutant heart started beating normally, and this beating continued. On the other hand, once the heart beating started, a limited region of the ventricle ruptured, though *flnc* was expressed in all myocardial cells. One reason for this tendency for a limited rupture region is that the ventricle was exposed to higher mechanical stress caused by contraction than was the atrium. Thus, this *zac* mutant phenotype indicates that the loss of filamin C may have weakened the mechanical strength of the heart. In accordance with this notion, we observed that the *zac* cardiomyocytes had an abnormally ruffled cell membrane surface, which is probably a consequence of failure of proper cell–cell adhesion, as previously described in the case of *in vitro* cultured cells (Borm et al., 2005). Moreover, TEM analysis revealed that fewer sarcomere bundles were attached to the intercalated disks, where the muscle sarcomeres are involved in establishing cell–cell adhesion. Based on all of our data taken together, we propose that the function of filamin C in the heart may be required for the integrity and stability of the cardiomyocytes.

Compared with the medaka *zac* mutant, the heart phenotype has not been highlighted in the mouse filamin C-deficient model (Dalkilic et al., 2006). This mouse is designed to generate a partial-loss-of-function model, which lacks only the repeats 20th–24th. The expression of a truncated filamin C was detected in this mouse model, especially at a higher level in heart than in skeletal muscle. Similar truncation mutations in *FLNA* have caused total- or partial-loss-of-function phenotypes in human patients (Feng and Walsh, 2004). Like *FLNA* and *FLNB* mutations (Krakow et al., 2004; Robertson et al., 2003), the position of the mutation may be responsible for variation in the phenotypes in *FLNC*. Recently, Duff et al. reported that mutations in the actin-binding domain of filamin C cause a distal myopathy, in which muscle pathology is totally different from the previous cases having myofibrillar myopathy, which is caused by mutations in either the rod or the dimerization domain of filamin C (Duff et al., 2011). In *zac* mutants, a nonsense mutation in the 15th repeat caused a marked reduction in the level of *flnc* mRNA, such that it was barely detectable in the heart (see Fig. 3F). In addition, translational knockdown by injecting MO revealed a cardiac phenotype similar to that of the *zac* mutant. Taken together, our present findings indicate that the *zac* mutation may represent complete disruption of the filamin C function, leading to severer phenotypes than those seen in the mouse model.

Function of filamin C in skeletal muscle

Since the expression of filamin C started at the onset of somitogenesis, we examined the effect of the *zac* mutation on muscle differentiation. The expressions of muscle differentiation markers were normal, and most of the muscle fibers showed a completely normal structure, based on the electron microscopic observations made at the early stage. However, muscle degeneration started in focal areas, and progressed, with the result being that a larger area became affected by the hatching stage. This progressive muscle phenotype reminded us of its similarity to the one in filamin C-deficient mice, where most fibers exhibited a normal sarcomeric structure, and only some fibers showed Z-disk abnormality. These results suggest that filamin C plays a role in the maintenance of the muscle structure rather than one in myofibrillogenesis in medaka as well as in mammals.

We observed the accumulation of γ-actin at MTJs in wild-type medaka embryos (see Fig. 8). In mammalian muscle fibers, γ-actin exclusively constitutes the subsarcolemmal actin-based cytoskeleton (Rybakova et al., 2000). The γ-actin filaments provide a structural support to muscle fibers by interacting with DGC and the integrin complex. In medaka embryos, DGC and integrin as well as filamin C were concentrated at the MTJs (Fig. 8). Filamin C interacts with both DGC and integrin (Gontier et al., 2005; Loo et al., 1998; Thompson et al., 2000). It was reported that filamin A, the homologue of filamin C, protects cells from mechanical stress by increasing the rigidity of the cortical actin cytoskeleton in non-muscle cells (D'Addario et al., 2001; D'Addario et al., 2003; Shifrin et al., 2009). Thus, it is most likely that filamin C is involved in the linkage system through its interaction with the actin cytoskeleton, DGC, and integrin at the MTJs. Actually, the γ-actin content was reduced and myofibrils were severely affected at the MTJ in *zac* mutants (Figs. 7D, F and 8). Moreover, sarcomere structures in zac mutants were more fragile to mechanical stress caused by muscle contraction (Fig. 9). From these results, we suggest that filamin C participates in the linkage system at the MTJs through the stabilization of γ-actin filaments, protecting sarcomere structures from mechanical stress. In addition, γ-actin is also localized at Z-disks (Nakata et al., 2001), as was filamin C observed presently. Our TEM observation revealed that Z-disks were absent in some myofibrils in the *zac* mutants in late stages and that the sarcolemma had detached from the myofibrils, suggesting another role for filamin C in the lateral connections between myofibrils or between myofibrils and the sarcolemma. Unlike the skeletal muscle, cardiac muscle did not show expression of γ-actin in medaka (data not shown), which is consistent with that γ-actin is expressed mainly in smooth muscle actin (Herman, 1993). Different mechanism and interacting partners with filamin C might be involved to retain the mechanical stability at the intercalated disk in cardiomyocytes.

Patients with mutations in either the rod or the dimerization domain of filamin C show large protein aggregates containing the filamin C itself and its interacting proteins, myotilin and Xin, as well as Z-disk-associated proteins, desmin and αB-crystallin, in the cytoplasm of their muscle fibers (Kley et al., 2007; Luan et al., 2010; Shatunov et al., 2009). Ectopic expression of DGC components in the cytoplasm is also observed. Also, it was demonstrated that the W2710X mutation disturbs the structural stability of filamin C protein, leading to perturbed dimerization (Lowe et al., 2007). As a consequence, it has been suggested that mutant filamin C becomes prone to form aggregates, recruiting its interacting proteins into these aggregates. On the other hand, we did not observe any protein aggregates or cytoplasmic expressions of DGC components in the *zac* mutant. Since the expression of mutant filamin C was remarkably decreased in *zac* mutants, it may have not affected the

localization of the interacting proteins. Instead of aggregates, large vacuoles and dilated sarcoplasmic reticulum were observed electron microscopically in cardiac and skeletal muscle fibers in the *zac* mutants (see Figs. 6H and 7J). These vacuoles, which consisted of a single membrane, did not contain any sarcomeric or membranous materials. These features are totally different from the rimmed vacuoles often seen in patients with the W2710X mutation. Non-rimmed vacuoles with strong PAS-positivity were also reported in these patients, but no accumulation of glycogen was seen in the vacuoles in the *zac* mutants. These vacuoles were not described in the mouse model of filamin C-deficiency, either. Although the presence of vacuoles and dilated sarcoplasmic reticula were described in a report on mechanically induced cell death (Kainulainen et al., 2002) or on animal models of collagen VI-deficiency myopathy, in which apoptosis is enhanced in the skeletal muscle (Irwin et al., 2003; Telfer et al., 2010), the level of apoptosis, as assessed by the TUNEL assay, was not altered in the *zac* mutants (data not shown). Furthermore, no nuclei showing features of apoptosis, such as chromatin condensation, were observed in them. Further studies are required to explain the mechanism of vacuole formation and sarcoplasmic reticulum dilatation.

In light of all of our data taken together, we propose a working hypothesis in which filamin C plays an essential role in maintaining the skeletal and cardiac muscle cell alignment and structure, which hypothesis would explain how these muscles can resist mechanical forces to retain the integrity and stability of their adhesion machineries. Filaminopathy patients frequently develop cardiomyopathy, but the cellular basis for the occurrence of these symptoms has been obscure. Therefore, our analysis using the medaka *zac* mutant offers a useful animal model for understanding the function of filamin C in the maintenance of the structural integrity of muscle cells. Moreover, it has not been proved yet that the function of filamin C is linked to the severe heart phenotype such as the rupture of heart chambers seen in humans. It is possible that filamin C may be associated with idiopathic cardiomyopathy. Further functional analyses may provide us a better understanding of the molecular mechanism of filamin C by which muscular tissues are maintained against mechanical stress.

Finally, regarding the medaka filamin C ortholog: FLNC (2 of 2), to find whether it is involved in Filamin C function in medaka, the further development of medaka genome research is required to confirm the whole genome structure of FLNC (2 of 2).

Supplementary materials related to this article can be found online at doi:10.1016/j.ydbio.2011.10.008.

Acknowledgments

We thank Y. Ishikawa (National Institute for Radiological Sciences, Japan) and members of the screening team for isolating mutants. We thank Y. Takahashi (Iwate Medical University) for heart sectioning and hematoxylin/eosin Y staining, as well as K. Inohaya and Y. Nakatani for their helpful support and discussions. We thank H. Yorifuji (Gunma University Graduate School of Medicine) for providing anti-γ-actin antibody. Hatching enzyme was obtained from National BioResource Project Medaka, Japan. This study was supported by the following sources: a grant-in-aid for scientific research from Japan Society for the Promotion of Science and grants from the programs Research on Psychiatric and Neurological Diseases and Mental Health; Research on Measures for Intractable Diseases; Health Labour Sciences Research Grants for Nervous and Mental Disorders (20B-12, 20B-13) from the Ministry of Health, Labor, and Welfare; and Intramural Research Grants (23-4, 23-5, 23-6) for Neurological and Psychiatric Disorders of NCNP.

References

Anastasi, G., Cutroneo, G., Gaeta, R., Di Mauro, D., Arco, A., Consolo, A., Santoro, G., Trimarchi, F., Favaloro, A., 2009. Dystrophin–glycoprotein complex and vinculin–talin–integrin system in human adult cardiac muscle. Int. J. Mol. Med. 23, 149–159.

Arahata, K., Ishiura, S., Ishiguro, T., Tsukahara, T., Suhara Y., Eguchi, C., Ishihara, T., Nonaka, I., Ozawa, E., Sugita, H., 1988. Immunostaining of skeletal and cardiac muscle surface membrane with antibody against Duchenne muscular dystrophy peptide. Nature 333, 861–863.

Baker, K.E., Parker, R., 2004. Nonsense-mediated mRNA decay: terminating erroneous gene expression. Curr. Opin. Cell Biol. 16, 293–299.

Bao, Z.Z., Lakonishok, M., Kaufman, S., Horwitz, A.F., 1993. Alpha 7 beta 1 integrin is a component of the myotendinous junction on skeletal muscle. J. Cell Sci. 106, 579–589.

Bassett, D.I., Bryson-Richardson, R.J., Daggett, D.F., Gautier, P., Keenan, D.G., Currie, P.D., 2003. Dystrophin is required for the formation of stable muscle attachments in the zebrafish embryo. Development 130, 5851–5860.

Bonnemann, C.G., Modi, R., Noguchi, S., Mizuno, Y., Yoshida, M., Gussoni, E., McNally, E.M., Duggan, D.J., Angelini, C., Hoffman, E.P., 1995. Beta-sarcoglycan (A3b) mutations cause autosomal recessive muscular dystrophy with loss of the sarcoglycan complex. Nat. Genet. 11, 266–273.

Borm, B., Requardt, R.P., Herzog, V., Kirfel, G., 2005. Membrane ruffles in cell migration: indicators of inefficient lamellipodia adhesion and compartments of actin filament reorganization. Exp. Cell Res. 302, 83–95.

Burkin, D.J., Kaufman, S.J., 1999. The alpha7beta1 integrin in muscle development and disease. Cell Tissue Res. 296, 183–190.

Campbell, K.P., 1995. Three muscular dystrophies: loss of cytoskeleton–extracellular matrix linkage. Cell 80, 675–679.

Cheng, L., Guo, X.F., Yang, X.Y., Chong, M., Cheng, J., Li, G., Gui, Y.H., Lu, D.R., 2006. Delta-sarcoglycan is necessary for early heart and muscle development in zebrafish. Biochem. Biophys. Res. Commun. 344, 1290–1299.

D'Addario, M., Arora, P.D., Ellen, R.P., McCulloch, C.A., 2003. Regulation of tension-induced mechanotranscriptional signals by the microtubule network in fibroblasts. J. Biol. Chem. 278, 53090–53097.

D'Addario, M., Arora, P.D., Fan, J., Ganss, B., Ellen, R.P., McCulloch, C.A., 2001. Cytoprotection against mechanical forces delivered through beta 1 integrins requires induction of filamin A. J. Biol. Chem. 276, 31969–31977.

Dalkilic, I., Schienda, J., Thompson, T.G., Kunkel, L.M., 2006. Loss of filaminC (FLNc) results in severe defects in myogenesis and myotube structure. Mol. Cell. Biol. 26, 6522–6534.

Duff, R.M., Tay, V., Hackman, P., Ravenscroft, G., McLean, C., Kennedy, P., Steinbach, A., Schoffler, W., van der Ven, P.F., Furst, D.O., Song, J., Djinovic-Carugo, K., Penttila, S., Raheem, O., Reardon, K., Malandrini, A., Gambelli, S., Villanova, M., Nowak, K.J., Williams, D.R., Landers, J.E., Brown Jr., R.H., Udd, B., Laing, N.G., 2011. Mutations in the N-terminal actin-binding domain of filamin C cause a distal myopathy. Am. J. Hum. Genet. 88, 729–740.

Ervasti, J.M., 2003. Costameres: the Achilles' heel of Herculean muscle. J. Biol. Chem. 278, 13591–13594.

Faulkner, G., Pallavicini, A., Comelli, A., Salamon, M., Bortoletto, G., Ievolella, C., Trevisan, S., Kojic, S., Dalla Vecchia, F., Laveder, P., Valle, G., Lanfranchi, G., 2000. FATZ, a filamin-, actinin-, and telethonin-binding protein of the Z-disc of skeletal muscle. J. Biol. Chem. 275, 41234–41242.

Feng, Y., Walsh, C.A., 2004. The many faces of filamin: a versatile molecular scaffold for cell motility and signalling. Nat. Cell Biol. 6, 1034–1038.

Gontier, Y., Taivainen, A., Fontao, L., Sonnenberg, A., van der Flier, A., Carpen, O., Faulkner, G., Borradori, L., 2005. The Z-disc proteins myotilin and FATZ-1 interact with each other and are connected to the sarcolemma via muscle-specific filamins. J. Cell Sci. 118, 3739–3749.

Granato, M., van Eeden, F.J., Schach, U., Trowe, T., Brand, M., Furutani-Seiki, M., Haffter, P., Hammerschmidt, M., Heisenberg, C.P., Jiang, Y.J., Kane, D.A., Kelsh, R.N., Mullins, M.C., Odenthal, J., Nusslein-Volhard, C., 1996. Genes controlling and mediating locomotion behavior of the zebrafish embryo and larva. Development 123, 399–413.

Gupta, V., Kawahara, G., Gundry, S.R., Chen, A.T., Lencer, W.I., Zhou, Y., Zon, L.I., Kunkel, L.M., Beggs, A.H., 2011. The zebrafish dag1 mutant: a novel genetic model for dystroglycanopathies. Hum. Mol. Genet. 20, 1712–1725.

Guyon, J.R., Mosley, A.N., Jun, S.J., Montanaro, F., Steffen, L.S., Zhou, Y., Nigro, V., Zon, L.I., Kunkel, L.M., 2005. Delta-sarcoglycan is required for early zebrafish muscle organization. Exp. Cell Res. 304, 105–115.

Guyon, J.R., Steffen, L.S., Howell, M.H., Pusack, T.J., Lawrence, C., Kunkel, L.M., 2007. Modeling human muscle disease in zebrafish. Biochim. Biophys. Acta 1772, 205–215.

Hartwig, J.H., Stossel, T.P., 1975. Isolation and properties of actin, myosin, and a new actinbinding protein in rabbit alveolar macrophages. J. Biol. Chem. 250, 5696–5705.

Hayashi, Y.K., Chou, F.L., Engvall, E., Ogawa, M., Matsuda, C., Hirabayashi, S., Yokochi, K., Ziober, B.L., Kramer, R.H., Kaufman, S.J., Ozawa, E., Goto, Y., Nonaka, I., Tsukahara, T., Wang, J.Z., Hoffman, E.P., Arahata, K., 1998. Mutations in the integrin alpha7 gene cause congenital myopathy. Nat. Genet. 19, 94–97.

Herman, I.M., 1993. Actin isoforms. Curr. Opin. Cell Biol. 5, 48–55.

Hoffman, E.P., Brown Jr., R.H., Kunkel, L.M., 1987. Dystrophin: the protein product of the Duchenne muscular dystrophy locus. Cell 51, 919–928.

Hyodo-Taguchi, Y., 1980. Establishment of inbred strains of the teleost, *Oryzias latipes*. Zool. Mag. 89, 283–301.

Inohaya, K., Yasumasu, S., Ishimaru, M., Ohyama, A., Iuchi, I., Yamagami, K., 1995. Temporal and spatial patterns of gene expression for the hatching enzyme in the teleost embryo, *Oryzias latipes*. Dev. Biol. 171, 374–385.

Inohaya, K., Yasumasu, S., Yasumasu, I., Iuchi, I., Yamagami, K., 1999. Analysis of the origin and development of hatching gland cells by transplantation of the embryonic shield in the fish, *Oryzias latipes*. Dev. Growth Differ. 41, 557–566.

Irwin, W.A., Bergamin, N., Sabatelli, P., Reggiani, C., Megighian, A., Merlini, L., Braghetta, P., Columbaro, M., Volpin, D., Bressan, G.M., Bernardi, P., Bonaldo, P., 2003.

Mitochondrial dysfunction and apoptosis in myopathic mice with collagen VI deficiency. Nat. Genet. 35, 367–371.
Ishikawa, Y., 1996. A recessive lethal mutation, tb, that bends the midbrain region of the neural tube in the early embryo of the medaka. Neurosci. Res. 24, 313–317.
Ishikawa, Y., 2000. Medakafish as a model system for vertebrate developmental genetics. Bioessays 22, 487–495.
Ishikawa, Y., Hyodo-Taguchi, Y., Aoki, K., Yasuda, T., Matsumoto, A., Sasanuma, M., 1999. Induction of mutations by ENU in the medaka germline. Fish Biol. J. Medaka 10, 27–29.
Iwamatsu, T., 2004. Stages of normal development in the medaka *Oryzias latipes*. Mech. Dev. 121, 605–618.
Kainulainen, T., Pender, A., D'Addario, M., Feng, Y., Lekic, P., McCulloch, C.A., 2002. Cell death and mechanoprotection by filamin A in connective tissues after challenge by applied tensile forces. J. Biol. Chem. 277, 21998–22009.
Kimura, T., Jindo, T., Narita, T., Naruse, K., Kobayashi, D., Shin, I.T., Kitagawa, T., Sakaguchi, T., Mitani, H., Shima, A., Kohara, Y., Takeda, H., 2004. Large-scale isolation of ESTs from medaka embryos and its application to medaka developmental genetics. Mech. Dev. 121, 915–932.
Kley, R.A., Hellenbroich, Y., van der Ven, P.F., Furst, D.O., Huebner, A., Bruchertseifer, V., Peters, S.A., Heyer, C.M., Kirschner, J., Schroder, R., Fischer, D., Muller, K., Tolksdorf, K., Eger, K., Germing, A., Brodherr, T., Reum, C., Walter, M.C., Lochmuller, H., Ketelsen, U.P., Vorgerd, M., 2007. Clinical and morphological phenotype of the filamin myopathy: a study of 31 German patients. Brain 130, 3250–3264.
Krakow, D., Robertson, S.P., King, L.M., Morgan, T., Sebald, E.T., Bertolotto, C., Wachsmann-Hogiu, S., Acuna, D., Shapiro, S.S., Takafuta, T., Aftimos, S., Kim, C.A., Firth, H., Steiner, C.E., Cormier-Daire, V., Superti-Furga, A., Bonafe, L., Graham Jr., J.M., Grix, A., Bacino, C.A., Allanson, J., Bialer, M.G., Lachman, R.S., Rimoin, D.L., Cohn, D.H., 2004. Mutations in the gene encoding filamin B disrupt vertebral segmentation, joint formation and skeletogenesis. Nat. Genet. 36, 405–410.
Lim, L.E., Duclos, F., Broux, O., Bourg, N., Sunada, Y., Allamand, V., Meyer, J., Richard, I., Moomaw, C., Slaughter, C., Tomé, F.M., Fardeau, M., Jackson, C.E., Beckmann, J.S., Campbell, K.P., 1995. Beta-sarcoglycan: characterization and role in limb-girdle muscular dystrophy linked to 4q12. Nat. Genet. 11, 257–265.
Linnemann, A., van der Ven, P.F., Vakeel, P., Albinus, B., Simonis, D., Bendas, G., Schenk, J.A., Micheel, B., Kley, R.A., Furst, D.O., 2010. The sarcomeric Z-disc component *myopodin is a multiadapter protein that interacts with filamin and alpha-actinin*. Eur. J. Cell Biol. 89, 681–692.
Loo, D.T., Kanner, S.B., Aruffo, A., 1998. Filamin binds to the cytoplasmic domain of the beta1-integrin. Identification of amino acids responsible for this interaction. J. Biol. Chem. 273, 23304–23312.
Lowe, T., Kley, R.A., van der Ven, P.F., Himmel, M., Huebner, A., Vorgerd, M., Furst, D.O., 2007. The pathomechanism of filaminopathy: altered biochemical properties explain the cellular phenotype of a protein aggregation myopathy. Hum. Mol. Genet. 16, 1351–1358.
Luan, X., Hong, D., Zhang, W., Wang, Z., Yuan, Y., 2010. A novel heterozygous deletion–insertion mutation (2695–2712 del/GTTTGT ins) in exon 18 of the filamin C gene causes filaminopathy in a large Chinese family. Neuromuscul. Disord. 20, 390–396.
Mayer, U., 2003. Integrins: redundant or important players in skeletal muscle? J. Biol. Chem. 278, 14587–14590.
Mayer, U., Saher, G., Fassler, R., Bornemann, A., Echtermeyer, F., von der Mark, H., Miosge, N., Poschl, E., von der Mark, K., 1997. Absence of integrin alpha 7 causes a novel form of muscular dystrophy. Nat. Genet. 17, 318–323.
Miosge, N., Klenczar, C., Herken, R., Willem, M., Mayer, U., 1999. Organization of the myotendinous junction is dependent on the presence of alpha7beta1 integrin. Lab. Invest. 79, 1591–1599.
Mizuno, Y., Noguchi, S., Yamamoto, H., Yoshida, M., Suzuki, A., Hagiwara, Y., Hayashi, Y.K., Arahata, K., Nonaka, I., Hirai, S., Ozawa, E., 1994. Selective defect of sarcoglycan complex in severe childhood autosomal recessive muscular dystrophy muscle. Biochem. Biophys. Res. Commun. 203, 979–983.
Nakata, T., Nishina, Y., Yorifuji, H., 2001. Cytoplasmic gamma actin as a Z-disc protein. Biochem. Biophys. Res. Commun. 286, 156–163.
Naruse, K., Fukamachi, S., Mitani, H., Kondo, M., Matsuoka, T., Kondo, S., Hanamura, N., Morita, Y., Hasegawa, K., Nishigaki, R., Shimada, A., Wada, H., Kusakabe, T., Suzuki, N., Kinoshita, M., Kanamori, A., Terado, T., Kimura, H., Nonaka, M., Shima, A., 2000. A detailed linkage map of medaka, *Oryzias latipes*: comparative genomics and genome evolution. Genetics 154, 1773–1784.
Nigro, V., de Sa Moreira, E., Piluso, G., Vainzof, M., Belsito, A., Politano, L., Puca, A.A., Passos-Bueno, M.R., Zatz, M., 1996. Autosomal recessive limb-girdle muscular dystrophy, LGMD2F, is caused by a mutation in the delta-sarcoglycan gene. Nat. Genet. 14, 195–198.
Noguchi, S., McNally, E.M., Ben Othmane, K., Hagiwara, Y., Mizuno, Y., Yoshida, M., Yamamoto, H., Bonnemann, C.G., Gussoni, E., Denton, P.H., Kyriakides, T., Middleton, L., Hentati, F., Ben Hamida, M., Nonaka, I., Vance, J.M., Kunkel, L.M., Ozawa, E., 1995. Mutations in the dystrophin-associated protein gamma-sarcoglycan in chromosome 13 muscular dystrophy. Science 270, 819–822.
Ohashi, K., Oshima, K., Tachikawa, M., Morikawa, N., Hashimoto, Y., Ito, M., Mori, H., Kuribayashi, T., Terasaki, A.G., 2005. Chicken gizzard filamin, retina filamin and cgABP260 are respectively, smooth muscle-, non-muscle- and pan-muscle-type isoforms: distribution and localization in muscles. Cell Motil. Cytoskeleton 61, 214–225.
Postel, R., Vakeel, P., Topczewski, J., Knoll, R., Bakkers, J., 2008. Zebrafish integrin-linked kinase is required in skeletal muscles for strengthening the integrin-ECM adhesion complex. Dev. Biol. 318, 92–101.
Roberds, S.L., Leturcq, F., Allamand, V., Piccolo, F., Jeanpierre, M., Anderson, R.D., Lim, L.E., Lee, J.C., Tomé, F.M., Romero, N.B., Fardeau, M., Beckmann, J.S., Kaplan, J.C., Campbell, K.P., 1994. Missense mutations in the adhalin gene linked to autosomal recessive muscular dystrophy. Cell 78, 625–633.
Robertson, S.P., Twigg, S.R., Sutherland-Smith, A.J., Biancalana, V., Gorlin, R.J., Horn, D., Kenwrick, S.J., Kim, C.A., Morava, E., Newbury-Ecob, R., Orstavik, K.H., Quarrell, O.W., Schwartz, C.E., Shears, D.J., Suri, M., Kendrick-Jones, J., Wilkie, A.O., 2003. Localized mutations in the gene encoding the cytoskeletal protein filamin A cause diverse malformations in humans. Nat. Genet. 33, 487–491.
Rybakova, I.N., Patel, J.R., Ervasti, J.M., 2000. The dystrophin complex forms a mechanically strong link between the sarcolemma and costameric actin. J. Cell Biol. 150, 1209–1214.
Samitt, C.E., Bonilla, E., 1990. Immunocytochemical study of dystrophin at the myotendinous junction. Muscle Nerve 13, 493–500.
Sehnert, A.J., Huq, A., Weinstein, B.M., Walker, C., Fishman, M., Stainier, D.Y., 2002. Cardiac troponin T is essential in sarcomere assembly and cardiac contractility. Nat. Genet. 31, 106–110.
Selcen, D., 2008. Myofibrillar myopathies. Curr. Opin. Neurol. 21, 585–589.
Selcen, D., Ohno, K., Engel, A.G., 2004. Myofibrillar myopathy: clinical, morphological and genetic studies in 63 patients. Brain 127, 439–451.
Shatunov, A., Olive, M., Odgerel, Z., Stadelmann-Nessler, C., Irlbacher, K., van Landeghem, F., Bayarsaikhan, M., Lee, H.S., Goudeau, B., Chinnery, P.F., Straub, V., Hilton-Jones, D., Damian, M.S., Kaminska, A., Vicart, P., Bushby, K., Dalakas, M.C., Sambuughin, N., Ferrer, I., Goebel, H.H., Goldfarb, L.G., 2009. In-frame deletion in the seventh immunoglobulin-like repeat of filamin C in a family with myofibrillar myopathy. Eur. J. Hum. Genet. 17, 656–663.
Shifrin, Y., Arora, P.D., Ohta, Y., Calderwood, D.A., McCulloch, C.A., 2009. The role of FilGAP–filamin A interactions in mechanoprotection. Mol. Biol. Cell 20, 1269–1279.
Shimizu, T., Matsumura, K., Sunada, Y., Mannen, T., 1989. Dense immunostainings on both neuromuscular and myotendon junction with an anti-dystrophin monoclonal antibody. Biomed. Res. 10, 405–409.
Steffen, L.S., Guyon, J.R., Vogel, E.D., Beltre, R., Pusack, T.J., Zhou, Y., Zon, L.I., Kunkel, L.M., 2007. *Zebrafish orthologs of human muscular dystrophy genes*. BMC Genomics 8, 79.
Stossel, T.P., Condeelis, J., Cooley, L., Hartwig, J.H., Noegel, A., Schleicher, M., Shapiro, S.S., 2001. Filamins as integrators of cell mechanics and signalling. Nat. Rev. Mol. Cell Biol. 2, 138–145.
Stossel, T.P., Hartwig, J.H., 1975. Interactions between actin, myosin, and an actin-binding protein from rabbit alveolar macrophages. Alveolar macrophage myosin Mg^{2+}-adenosine triphosphatase requires a cofactor for activation by actin. J. Biol. Chem. 250, 5706–5712.
Summers, A.P., Koob, T.J., 2002. The evolution of tendon – morphology and material properties. Comp. Biochem. Physiol. A Mol. Integr. Physiol. 133, 1159–1170.
Telfer, W.R., Busta, A.S., Bonnemann, C.G., Feldman, E.L., Dowling, J.J., 2010. Zebrafish models of collagen VI-related myopathies. Hum. Mol. Genet. 19, 2433–2444.
Thompson, T.G., Chan, Y.M., Hack, A.A., Brosius, M., Rajala, M., Lidov, H.G., McNally, E.M., Watkins, S., Kunkel, L.M., 2000. Filamin 2 (FLN2): a muscle-specific sarcoglycan interacting protein. J. Cell Biol. 148, 115–126.
van der Flier, A., Gaspar, A.C., Thorsteinsdottir, S., Baudoin, C., Groeneveld, E., Mummery, C.L., Sonnenberg, A., 1997. Spatial and temporal expression of the beta1D integrin during mouse development. Dev. Dyn. 210, 472–486.
van der Ven, P.F., Obermann, W.M., Lemke, B., Gautel, M., Weber, K., Furst, D.O., 2000a. Characterization of muscle filamin isoforms suggests a possible role of gamma-filamin/ABP-L in sarcomeric Z-disc formation. Cell Motil. Cytoskeleton 45, 149–162.
van der Ven, P.F., Wiesner, S., Salmikangas, P., Auerbach, D., Himmel, M., Kempa, S., Hayess, K., Pacholsky, D., Taivainen, A., Schroder, R., Carpen, O., Furst, D.O., 2000b. Indications for a novel muscular dystrophy pathway. gamma-filamin, the muscle-specific filamin isoform, interacts with myotilin. J. Cell Biol. 151, 235–248.
Vorgerd, M., van der Ven, P.F., Bruchertseifer, V., Lowe, T., Kley, R.A., Schroder, R., Lochmuller, H., Himmel, M., Koehler, K., Furst, D.O., Huebner, A., 2005. A mutation in the dimerization domain of filamin c causes a novel type of autosomal dominant myofibrillar myopathy. Am. J. Hum. Genet. 77, 297–304.
Wada, H., Shimada, A., Fukamachi, S., Naruse, K., Shima, A., 1998. Sex-linked inheritance of the lf locus in the medaka fish (*Oryzias latipes*). Zoolog. Sci. 15 123–126.
Watkins, S.C., Hoffman, E.P., Slayter, H.S., Kunkel, L.M., 1988. Immunoelectron microscopic localization of dystrophin in myofibres. Nature 333, 863–866.
Wittbrodt, J., Shima, A., Schartl, M., 2002. Medaka—a model organism from the far East. Nat. Rev. Genet. 3, 53–64.
Xu, X., Meiler, S.E., Zhong, T.P., Mohideen, M., Crossley, D.A., Burggren, W.W., Fishman, M.C., 2002. Cardiomyopathy in zebrafish due to mutation in an alternatively spliced exon of titin. Nat. Genet. 30, 205–209.
Yoshida, M., Hama, H., Ishikawa-Sakurai, M., Imamura, M., Mizuno, Y., Araishi, K., Wakabayashi-Takai, E., Noguchi, S., Sasaoka, T., Ozawa, E., 2000. Biochemical evidence for association of dystrobrevin with the sarcoglycan–sarcospan complex as a basis for understanding sarcoglycanopathy. Hum. Mol. Genet. 9, 1033–1040.

Available online at www.sciencedirect.com

SciVerse ScienceDirect

Neuromuscular Disorders 22 (2012) 149–151

www.elsevier.com/locate/nmd

Case report

A novel mutation in the *LMNA* gene causes congenital muscular dystrophy with dropped head and brain involvement

Ayako Hattori [a], Hirofumi Komaki [a,*], Masao Kawatani [b], Hiroshi Sakuma [a], Yoshiaki Saito [a], Eiji Nakagawa [a], Kenji Sugai [a], Masayuki Sasaki [a], Yukiko K. Hayashi [c], Ikuya Nonaka [a,c], Ichizo Nishino [c]

[a] *Department of Child Neurology, National Center Hospital, National Center of Neurology and Psychiatry (NCNP), Kodaira, Tokyo, Japan*
[b] *Department of Pediatrics, Faculty of Medical Sciences, University of Fukui, Fukui, Japan*
[c] *Department of Neuromuscular Research, National Institute of Neuroscience, NCNP, Kodaira, Tokyo, Japan*

Received 4 May 2011; received in revised form 17 July 2011; accepted 24 August 2011

Abstract

We describe a 22-month-old girl with axial muscle and diaphragmatic weakness as well as motor developmental delay without mental retardation. The striking clinical feature was a dropped head, although she could walk unaided. T2/FLAIR brain MRI revealed a focal abnormality with high signal intensity in the white matter including U-fibers. A muscle biopsy showed active necrotic and regenerative processes. These distinct clinical findings prompted a mutational analysis of the *lamin A* (*LMNA*) gene, and we identified a novel heterozygous mutation in *LMNA* (c.1330_1338dup9). This is the first report of an Asian patient with *LMNA*-related congenital muscular dystrophy (L-CMD) and a dropped head.

Keywords: A-type lamin; *LMNA*; L-CMD; Congenital muscular dystrophy; Dropped head; Brain abnormality

1. Introduction

The *LMNA* gene encoding A-type lamins that are nuclear envelope proteins is located on chromosome 1q11–q23. Mutations in *LMNA* are associated with various diseases, including autosomal dominant and recessive Emery–Dreifuss muscular dystrophy, limb-girdle muscular dystrophy type 1B, cardiomyopathy with conduction defects, familial partial lipodystrophy, Charcot-Marie-Tooth disease type 2B and premature aging syndromes [1]. *LMNA*-related congenital muscular dystrophy (L-CMD) characterized by severe axial muscle weakness with a dropped head has recently been described [2]. We describe the first Asian patient with L-CMD and a dropped head associated with a novel duplication mutation in *LMNA*.

2. Patient

A 22-month-old Japanese girl was the third child of healthy and non-consanguineous parents. Neuromuscular diseases were not evident in the family history. The patient was born at term with no abnormalities during the pregnancy and neonatal period. Psychomotor development was normal except for poor head control. She sat upright at 9 months of age and walked unaided at 13 months.

A neurological examination at the age of 22 months revealed severe axial muscle weakness predominantly in the neck. She had a proximal dominant muscle weakness, used the Gowers' maneuver to stand up, and had difficulty in raising her arms. She could walk independently with a

* Corresponding author. Address: Department of Child Neurology, National Center Hospital, NCNP, Ogawahigashi 4-1-1, Kodaira, Tokyo 187-8551, Japan.
E-mail address: komakih@ncnp.go.jp (H. Komaki).

0960-8966/$ - see front matter © 2011 Elsevier B.V. All rights reserved.
doi:10.1016/j.nmd.2011.08.009

dropped-head posture, but often fell, and was unable to run. Diaphragmatic weakness was observed by fluoroscopy, and transcutaneous blood gas monitoring showed hypercapnia during sleep (Fig. 1B). Deep tendon reflexes were absent. No joint contractures and spinal rigidity were evident.

Her serum CK level was 1317 IU/L (normal <200 IU/L), and electromyography showed myopathic patterns with normal motor and sensory nerve conduction. T2-weighted and FLAIR MRI of the brain showed areas of focal high signal intensity in the white matter including U-fibers (Fig. 2). Findings of electrocardiography and echocardiography were normal. A muscle biopsy taken from the biceps brachii at age 22 months showed myopathic changes with necrotic and regenerating fibers (Fig. 1). Immunohistochemical assessment identified positive staining for dystrophin, sarcoglycans, alpha-dystroglycan, emerin, merosin and collagen VI. Mutational analysis of *LMNA* revealed a heterozygous c.1330_1338dup9 (p.E444_D446dup) in exon 7. This duplication was not found in 100 control Japanese DNA samples.

3. Discussion

Reports of L-CMD with a dropped head are rare, and all of them have been from Europe [2–6]. Here we describe the first Asian patient with L-CMD accompanied by a dropped head caused by a novel mutation in the *LMNA*. The muscle weakness in this patient was distinctive in that she was unable to steadily hold up her head and crawl, although she could walk independently. Due to the characteristic muscle involvement with dystrophic muscle pathol-

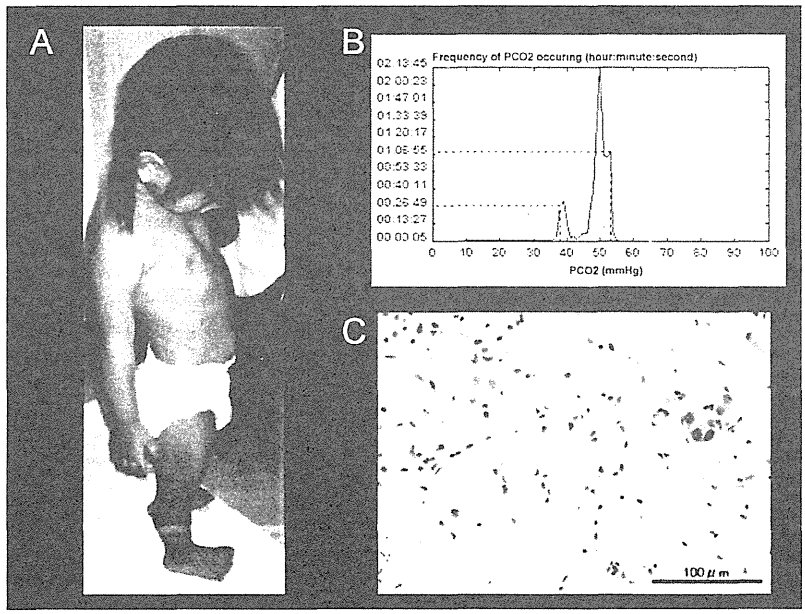

Fig. 1. Patient at age 22 months shows dropped head (A). She can stand and walk independently. Transcutaneous blood gas monitoring of PCO_2 during sleep (B). Muscle biopsy stained with hematoxylin and eosin (C). Necrotic, regenerating and other fibers remarkably vary in size.

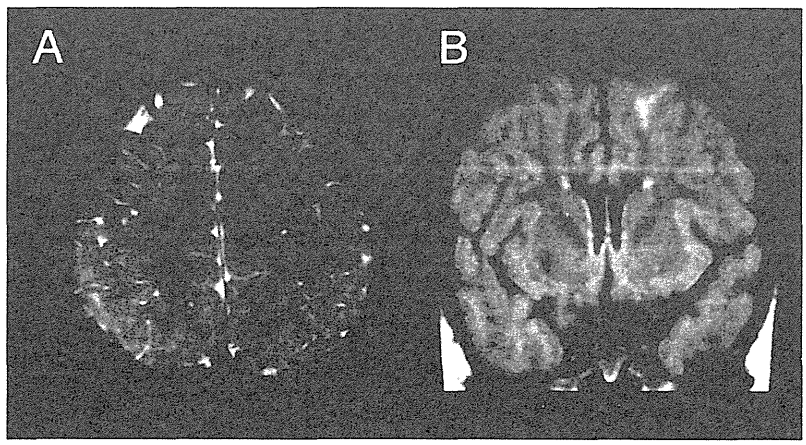

Fig. 2. MRI image of brain. Axial T2 weighted (A) and coronal FLAIR (B) images show focal high signals in white matter including U-fibers.

ogy, we performed a mutational analysis of the *LNMA* and discovered a novel 9-bp duplication that produced a duplication of three amino acids (p.E444_D446dup). A heterozygous missense mutation in *LMNA* is the usual cause of L-CMD and this is the first report of L-CMD caused by an in-frame duplication mutation.

Quijano-Roy et al. clinically subdivided L-CMD in 15 patients into severe and dropped-head types [2]. Nine patients with the dropped-head type acquired independent ambulation between the ages of 13 months and 2.5 years. However, most of them lost the ability to walk within a few years. Respiratory involvement was also evident in the eight of the patients with dropped-head type, and seven of them required non-invasive positive pressure ventilation. Cardiac arrhythmia was another important clinical finding in four of the 15 patients, and one suddenly died despite the outcomes of cardiac studies being normal [2]. Our patient was classified as having the dropped-head type of L-CMD with a diaphragmatic weakness and mild hypercapnia that indicated respiratory insufficiency. Considering published clinical information about L-CMD, respiratory and cardiac management is crucial, because respiratory failure and/or arrhythmia may develop later in life. Polysomnography and 24-h Holter electrocardiography will be performed as soon as our patient is old enough to cooperate, and ventilatory support will be provided if the respiratory insufficiency progress.

Brain MRI revealed focal white matter changes in our patient. Changes in the white matter of the brain without molecular data have been associated with Emery–Dreifuss muscular dystrophy [7], but brain involvement has not been associated with *LMNA* mutations until now. Such MRI findings might have occurred independently. Further studies and careful follow up of central nervous system involvement are required for patients with *LMNA* mutations.

References

[1] Worman HJ, Bonne G. "Laminopathies": a wide spectrum of human diseases. Exp Cell Res 2007;313:2121–33.
[2] Quijano-Roy S, Mbieleu B, Bönnemann CG, et al.. De novo LNMA mutations cause a new form of congenital muscular dystrophy. Ann Neurol 2008;64:177–86.
[3] D'Amico A, Haliloglu G, Richard P, et al.. Two patients with 'Dropped head syndrome' due to mutations in LMNA or SEPN1 genes. Neuromuscul Disord 2005;15:521–4.
[4] Makri S, Clarke NF, Richard P, et al.. Germinal mosaicism for *LMNA* mimics autosomal recessive congenital muscular dystrophy. Neuromuscul Disord 2009;19:26–8.
[5] Kirschner J, Brune T, Wehnert M, et al.. p.S143F mutation in lamin A/C: a new phenotype combining myopathy and progeria. Ann Neurol 2005;57:148–51.
[6] Mercuri E, Poppe M, Quinlivan R, et al.. Extreme variability of phenotype in patients with an identical missense mutation in the lamin A/C gene: from congenital onset with severe phenotype to milder classic Emery-Dreifuss variant. Arch Neurol 2004;61:690–4.
[7] Semnic R, Vucurevic G, Kozic D, et al.. Emery-Dreiffus muscular dystrophy: MR imaging and spectroscopy in the brain and skeletal muscle. AJNR Am J Neuroradiol 2004;25:1840–2.

The American Journal of Pathology, Vol. 180, No. 4, April 2012

DOI: 10.1016/j.ajpath.2011.12.040

Molecular Pathogenesis of Genetic and Inherited Diseases

In Vivo Characterization of Mutant Myotilins

Etsuko Keduka,* Yukiko K. Hayashi,* Sherine Shalaby,* Hiroaki Mitsuhashi,*† Satoru Noguchi,* Ikuya Nonaka,* and Ichizo Nishino*

From the Department of Neuromuscular Research, National Institute of Neuroscience, National Center of Neurology and Psychiatry, Tokyo, Japan; and the Division of Genetics,† Children's Hospital Boston, Harvard Medical School, Boston, Massachusetts*

Myofibrillar myopathy (MFM) is a group of disorders that are pathologically defined by the disorganization of the myofibrillar alignment associated with the intracellular accumulation of Z-disk–associated proteins. MFM is caused by mutations in genes encoding Z-disk–associated proteins, including myotilin. Although a number of MFM mutations have been identified, it has been difficult to elucidate the precise roles of the mutant proteins. Here, we present a useful method for the characterization of mutant proteins associated with MFM. Expression of mutant myotilins in mouse tibialis anterior muscle by *in vivo* electroporation recapitulated both the pathological changes and the biochemical characteristics observed in patients with myotilinopathy. In mutant myotilin-expressing muscle fibers, myotilin aggregates and is costained with polyubiquitin, and Z-disk–associated proteins and myofibrillar disorganization were commonly seen. In addition, the expressed S60C mutant myotilin protein displayed marked detergent insolubility in electroporated mouse muscle, similar to that observed in human MFM muscle with the same mutation. Thus, *in vivo* electroporation can be a useful method for evaluating the pathogenicity of mutations identified in MFM. *(Am J Pathol 2012, 180: 1570–1580; DOI: 10.1016/j.ajpath.2011.12.040)*

Myofibrillar myopathy (MFM) is a group of neuromuscular diseases with common morphological features such as disorganized myofibrillar alignment and accumulation of Z-disk–associated proteins.[1] Mutations in genes encoding Z-disk–associated proteins are known to cause MFM. Disease-associated mutations have been identified in six genes, including myotilin, desmin, αB-crystallin, ZASP, filamin C, and BAG3.[2,3] Elucidation of their pathogenicity, however, is sometimes difficult.

Myotilin (myofibrillar protein with titin-like immunoglobulin domains) is a 57-kDa protein with 10 exons encoded by the myotilin gene (*MYOT*) on chromosome 5q31. Myotilin consists of a unique serine-rich domain at the N-terminus and two Ig-like domains at the C-terminus.[4–7] Myotilin is highly expressed in skeletal and cardiac muscle, and localizes to the Z-disk,[4] which plays important roles in sarcomere assembly, actin filament stabilization, and muscle force transmission.[8,9] Myotilin interacts with several Z-disk–associated proteins, including α-actinin,[4] filamin C,[10,11] FATZ,[11] ZASP,[12] and MuRF ubiquitin ligase.[13] Myotilin also interacts with actin monomers and filaments through its Ig-like domains, which also mediate homodimerization.[14] Previous studies have shown that myotilin can bundle actin filaments *in vitro*, acting alone or in collaboration with α-actinin and filamin C.[4,14,15] Thus, myotilin is thought to play a role in anchoring and stabilizing actin filaments at the Z-disk, and is involved in the organization and maintenance of Z-disk integrity.[12] Missense mutations in *MYOT* have been associated with MFM,[16–18] limb girdle muscular dystrophy type 1A,[17,19,20] and distal myopathy.[21,22] We have previously identified a mutation p.Arg405Lys (R405K) in exon 9 in the second Ig-like domain of myotilin. The R405K mutant myotilin exhibited defective homodimerization and decreased interaction with α-actinin in a yeast 2-hybrid (Y2H) system.[23] All of the other previously reported *MYOT* mutations are located in exon 2 [14,16–18,24], with p.Ser60Cys (S60C) being one of the most common mutations. The pathogenic effects of *MYOT* mutations and

Supported by a Grant-in-Aid for Scientific Research from the Japan Society for the Promotion of Science: a Comprehensive Research on Disability Health and Welfare (20B-12, 20B-13) award from the Ministry of Health, Labor and Welfare; a Research on Intractable Diseases award from the Ministry of Health, Labor and Welfare; an Intramural Research Grant (23-4, 23-5, 23-6) for Neurological and Psychiatric Disorders, National Center of Neurology and Psychiatry; and a grant from the Japan Foundation for Neuroscience and Mental Health.

Accepted for publication December 29, 2011.

Supplemental material for this article can be found at *http://ajp.amjpathol.org* or at doi: 10.1016/j.ajpath.2011.12.040.

Address reprint requests to Yukiko K. Hayashi, M.D, Ph.D., Department of Neuromuscular Research, National Institute of Neuroscience, National Center of Neurology and Psychiatry, 4-1-1 Ogawahigashicho, Kodaira, Tokyo, 187-8502, Japan. E-mail: hayasi_y@ncnp.go.jp.

the disease mechanism involved remain poorly understood.

Model animals, such as transgenic mice, have contributed to understanding of the critical pathogenic events in MFM.[25–27] Some MFMs, including myotilinopathies, are late-onset and slowly progressive diseases.[1,3] To reproduce clinical and pathological features in model animals for such late-onset mild myopathy is both labor intensive and time consuming. Among the 10 missense mutations identified to date in patients with myotilinopathy,[14,16–18,23,24] only the Thr57Ile (T57I) mutation reproduces the pathological changes in transgenic mice after 12 months of age.[28] To screen for candidate mutations in MFM, a new method is required for demonstrating the pathogenicity of mutations. In the present study, we expressed mutant myotilin in mouse muscle by *in vivo* electroporation and were able to easily reproduce pathological changes similar to those observed in skeletal muscle from patients with *MYOT* mutations.

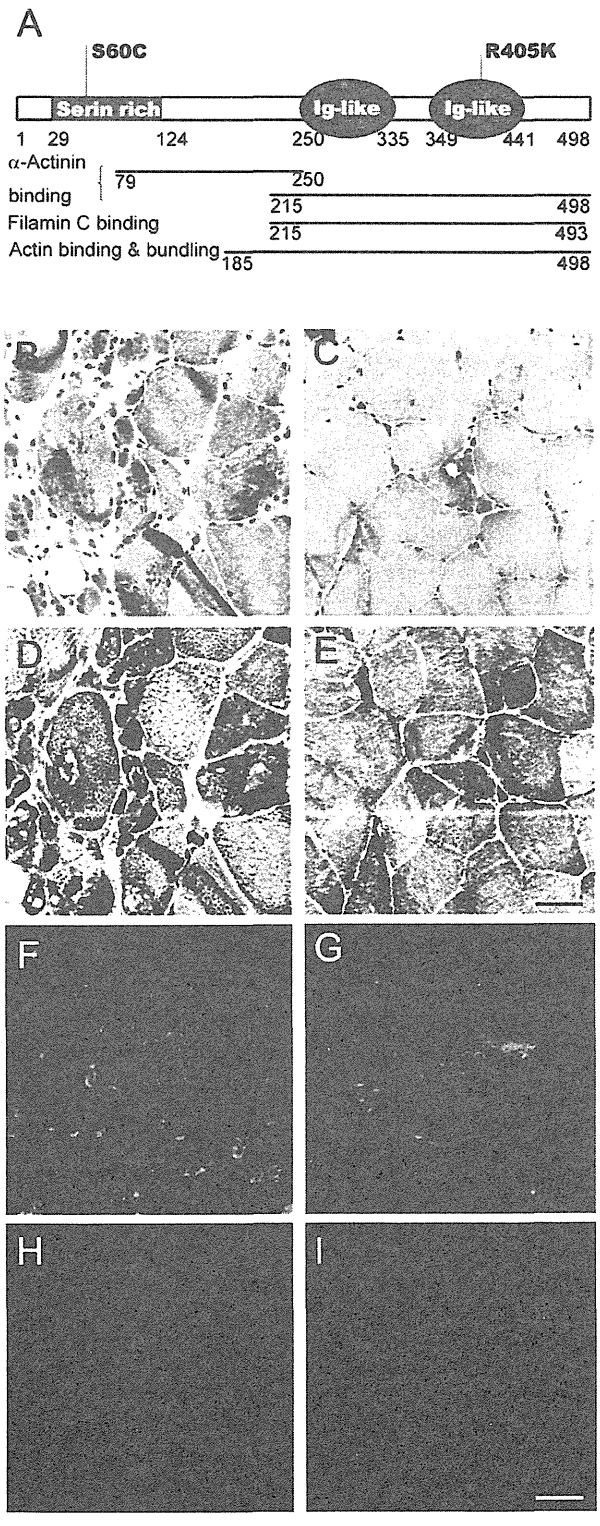

Materials and Methods

Clinical Materials

All clinical materials used in this study were obtained for diagnostic purposes with written informed consent. The studies were approved by the Ethical Committee of the National Center of Neurology and Psychiatry.

Genetic Analysis

Genomic DNA was isolated from peripheral lymphocytes or muscle specimens of patients, using standard techniques. Sequencing and mutation analysis of *MYOT* were performed as described previously.[23]

Plasmid Construction

We cloned full-length human myotilin cDNA and generated mutant myotilin (mMYOT) by site-directed mutagenesis, as described previously.[23] A C→G substitution at nucleotide position 179 and a G→A substitution at nucleotide 1214 were introduced to obtain p.S60C and p.R405K, respectively. A schematic of the location of these mutations in the structure of the myotilin protein is given in Figure 1A. For expression in mammalian cells, cDNAs of wild-type myotilin (wtMYOT) or mMYOT (S60C or R405K) were subcloned into pCMV-Myc vector (Ta-

Figure 1. Myotilin mutations and histopathological findings in myotilinopathy patients. **A:** Myotilin structure and disease-related mutations. p.Ser60Cys (S60C) is located in the serine-rich domain and p.Arg405Lys (R405K) is located in the second immunoglobulin (Ig)-like domain of myotilin. **B–I:** Pathological changes in muscles from patient 1 with *MYOT* S60C (**B**, **D**, **F**, and **H**) and from patient 2 with *MYOT* R405K (**C**, **E**, **G**, and **I**). **B:** Modified Gömöri trichrome (mGT) staining of biopsied skeletal muscle from patient 1 revealed markedly degenerated fibers with many spheroid protein inclusions (**arrows**). Some fibers had rimmed vacuoles (**arrowhead**). **C:** mGT staining of biopsied skeletal muscle from patient 2 revealed scattered fibers with rimmed vacuoles (**arrowhead**). **D:** NADH tetrazolium reductase (NADH-TR) staining of the serial section shown in **B** revealed markedly disorganized intermyofibrillar networks (**arrows**). **E:** NADH-TR staining of the serial section shown in **C** revealed disorganized intermyofibrillar networks (**arrow**). **F–I:** Coimmunostaining of muscles from patients using anti-myotilin (green) and anti-polyubiquitin (red) antibodies. **F:** Large accumulations of myotilin were observed in many fibers in patient 1. **G:** Small accumulations of myotilin were seen in some fibers in patient 2. Myotilin aggregates were positive for polyubiquitin in both patient 1 (**H**) and patient 2 (**I**). Scale bars: 50 μm (**B–E**); 20 μm (**F–I**).

kara Bio, Shiga, Japan). All constructs were verified by sequencing. Primer sequences are available on request.

Cell Culture, Transfection, and Immunocytochemical Analysis

C2C12 murine myoblast cells (American Type Culture Collection, Manassas, VA) were cultured in Dulbecco's modified Eagle's medium (Sigma-Aldrich, St. Louis, MO) supplemented with 10% fetal bovine serum (Invitrogen, Carlsbad, CA) at 37°C in a humidified atmosphere of 5% carbon dioxide. The cells were transiently transfected using FuGENE HD transfection reagent (Roche Diagnostics, Indianapolis, IN), according to the manufacturer's instructions. Forty-eight hours after transfection, the cells were fixed in 4% paraformaldehyde, permeabilized with 0.5% Triton-X 100, and costained with anti-Myc antibody (Sigma-Aldrich) and rhodamine-labeled phalloidin (Wako Pure Chemical Industries, Osaka, Japan) to detect transfected myotilin and actin filaments, respectively, according to standard protocol.[29]

In Vivo *Electroporation*

ICR mice were purchased from CLEA Japan (Fuji, Shizuoka, Japan). Animals were handled in accordance with the guidelines established by the Ethical Review Committee on the Care and Use of Rodents in the National Institute of Neuroscience, National Center of Neurology and Psychiatry. All mouse experiments were approved by the Committee. Five-week-old male ICR mice were anesthetized with diethyl ether, and the tibialis anterior (TA) muscles of mice were injected with 80 μg of purified Myc-tagged myotilin plasmid DNA. wtMYOT was injected to one side of TA muscle and mMYOT (S60C or R405K) was injected to the other side of TA muscle. *In vivo* transfection was performed using a square-wave electroporator (CUY-21SC; Nepa Gene, Ichikawa, Japan). A pair of electrode needles was inserted into the muscle to a depth of 3 mm to encompass the DNA injection sites. Each injected site was administered with three consecutive 50 ms-long pulses at the required voltage (50 to 90 V) to yield a current of 150 mA. After a 1-second interval, three consecutive pulses of the opposite polarity were administered. At 7 or 14 days after electroporation, mice were sacrificed by cervical dislocation, and TA muscles were isolated.

Histochemical and Immunohistochemical Analyses

Biopsied human muscles or electroporated mouse TA muscles were frozen in isopentane cooled in liquid nitrogen. Serial 10-μm cryosections were stained with modified Gömöri trichrome (mGT) and NADH-tetrazolium reductase (NADH-TR) and were subjected to a battery of histochemical methods. Immunohistochemistry was performed on serial 6-μm cryosections, as described previously.[29]

Antibodies

The primary antibodies used in this study were as follows: actin (Kantoukagaku, Tokyo, Japan), α-actinin (Sigma-Aldrich), BAG3 (Abcam, Tokyo, Japan), αB-crystallin (StressGen Biotechnologies, Victoria, BC, Canada), desmin (PROGEN Biotechnik, Heidelberg, Germany), filamin C (kindly provided by A.H. Beggs),[30] c-Myc (Sigma-Aldrich), c-Myc (PROGEN Biotechnik), myotilin (Proteintech Group, Chicago, IL), polyubiquitinated protein (Biomol International-Enzo Life Sciences, Plymouth Meeting, PA), GAPDH (Advanced ImmunoChemical, Long Beach, CA), and horseradish peroxidase-labeled anti-c-Myc antibody (Santa Cruz Biotechnology, Santa Cruz, CA).

Evaluation of Aggregates

Histochemical and immunohistochemical analyses were performed on cryosections of electroporated muscles sectioned at 500-μm intervals. The section containing the highest number of Myc-positive fibers (>100 fibers) was used. Myc-positive granules >1 μm in diameter were defined as aggregates. The Myc-positive fibers containing Myc-positive aggregates were counted among all Myc-positive fibers. Five mice each from the wtMYOT-, mMYOT S60C-, and mMYOT R405K-expressing groups were examined. To compare the number and size of Myc-positive aggregates per fiber, we measured the number and area of Myc-positive aggregates in 30 myofibers from each specimen using ImageJ software version 1.43 (NIH, Bethesda, MD). The results are presented as bar graphs (±SD) and histograms. Fifteen serial sections were immunoblotted to measure the amounts of electroporated Myc-tagged myotilin protein.

Electron Microscopy

For electron microscopy, cryosections (25 μm thick) of biopsied muscle with the S60C mutation (patient 1) were fixed with 2% glutaraldehyde in 100 mmol/L cacodylate buffer for 15 minutes on ice. After a shaking with a mixture of 4% osmium tetroxide, 1.5% lanthanum nitrate, and 200 mmol/L s-collidine for 1 to 2 hours, samples were embedded in epoxy resin. TA muscles of 5-week-old ICR mice were coelectroporated with pEGFP-C1 plasmid (Clontech, Tokyo, Japan), which encodes enhanced green fluorescent protein (EGFP), and with either Myc-wtMYOT or Myc-mMYOT (S60C or R405K) plasmid (40 μg each). As a control, pEGFP-C1 plasmid was electroporated alone. TA muscles were isolated 7 and 14 days after electroporation. EGFP-positive regions were trimmed under a fluorescence microscope and fixed with 2% glutaraldehyde in 100 mmol/L cacodylate buffer for 3 hours. After a shaking with a mixture of 4% osmium tetroxide, 1.5% lanthanum nitrate, and 200 mmol/L s-collidine for 2 to 3 hours, samples were embedded in epoxy resin. Semithin sections (1 μm thick) were stained with Toluidine Blue. Ultrathin sections (100 nm thick) were stained with uranyl acetate and lead citrate, and were analyzed at 120 kV using a Tecnai Spirit transmission electron microscope (FEI, Hillsboro, OR).

Solubility and Immunoblot Assay

To examine solubility of mutant myotilin, we used frozen biopsied muscles from human control subjects and from the two myotilinopathy patients, as well as TA muscles of six mice each from the wtMYOT-, mMYOT S60C-, and mMYOT R405K-expressing groups, at 14 days after electroporation. The 1.25-mm^3 specimens of muscle were lysed and homogenized in 150 μL of radioimmunoprecipitation assay buffer containing 50 mmol/L Tris-HCl (pH 7.5), 150 mmol/L NaCl, 1 mmol/L EDTA (pH 8.0), 1% Nonidet P-40, 0.5% sodium deoxycholate, 0.1% SDS, and Roche complete protease inhibitor cocktail (Roche Diagnostics). The lysates were incubated at 4°C for 20 minutes with gentle rotation, and then centrifuged at 15,000 × *g* at 4°C for 20 minutes. The supernatants and precipitates were collected, and the protein concentrations of the supernatants were determined using a protein assay kit (Bio-Rad Laboratories, Hercules, CA). Immunoblotting of the supernatant (detergent-soluble) and precipitate (detergent-insoluble) fractions was performed, as described previously.[23] Glyceraldehyde 3-phosphate dehydrogenase (GAPDH) was used as an internal standard. Immunoreactive complexes on the membranes were detected using enhanced chemiluminescence ECL Plus detection reagent (GE Healthcare, Chalfont St Giles, UK). Insolubility index was calculated as the ratio of the quantity of insoluble protein to the total quantity of proteins (the sum of soluble and insoluble proteins).

Immunoprecipitation

The 5-mm^3 specimens of frozen electroporated mouse muscles isolated at 14 days after electroporation were lysed and homogenized in 0.6 mL of radioimmunoprecipitation assay buffer. The lysates were incubated at 4°C for 20 minutes with gentle rotation, and then centrifuged at 15,000 × *g* at 4°C for 20 minutes. The supernatants were collected, and their protein concentrations were adjusted using a protein assay kit (Bio-Rad Laboratories). Immunoprecipitation was performed as described previously,[23] with agarose-conjugated anti-Myc antibody (Santa Cruz Biotechnology).

Statistical Analysis

Differences between wtMYOT-, mMYOT S60C-, and mMYOT R405K-expressing mice were analyzed with GraphPad Prism version 5 (GraphPad Software, La Jolla, CA). Comparisons among groups were performed by one-way analysis of variance with post hoc Tukey's analysis. Data are expressed as means ± SD.

Results

Mutation Screening and Histochemical Analyses of Muscles from Patients

We performed *MYOT* mutation screening in MFM patients and identified two patients with mutations. Patient 1, harboring a *MYOT* c.179C→G (p.S60C) mutation in exon 2, was a 63-year-old woman with a 6-year-long history of slowly progressive limb muscle weakness. Her mother (deceased) had had muscle weakness. The patient had difficulty in climbing stairs without support, and could not walk for long distances. Her serum creatine kinase level was elevated to 734 IU/L (reference, <200 IU/L). A biopsied specimen from the rectus femoris muscle showed marked variation in fiber size, with some necrotic fibers. Clusters of degenerated fibers with abnormal cytoplasmic inclusions were observed; some fibers with rimmed vacuoles were also seen (Figure 1B). Intermyofibrillar networks were markedly disorganized (Figure 1D). Under electron microscopy, electron-dense materials and cytoplasmic amorphous inclusions of various sizes were seen in some fibers (see Supplemental Figure S1 at *http://ajp.amjpathol.org*). Patient 2 was a 57-year-old woman harboring a *MYOT* c.1214G→A (p.R405K) mutation in exon 9. Detailed clinical symptoms have been described previously.[23] In brief, this patient had a 16-year-long history of slowly progressive proximal limb muscle weakness. Her serum creatine kinase level was mildly elevated (385 IU/l). A specimen from the vastus lateralis muscle showed marked variation in fiber size, scattered fibers with internal nuclei, and small angular fibers. Some fibers with rimmed vacuoles were seen (Figure 1C), and intermyofibrillar networks were disorganized (Figure 1E). Immunohistochemical analysis of muscle specimens from both patients revealed scattered fibers with strong immunoreactive accumulations of myotilin (Figure 1, F and G), which costained with polyubiquitin (Figure 1, H and I), α-B crystallin, BAG3, actin, desmin, and filamin C (see Supplemental Figure S2 at *http://ajp.amjpathol.org*).

Mutant Myotilin Does Not Aggregate in Cultured Cells

To examine the aggregation of mutant myotilins in cultured cells, C2C12 murine myoblasts were transfected with Myc-tagged wtMYOT (Myc-wtMYOT) or Myc-tagged mMYOT (Myc-mMYOT S60C or R405K). After 48 hours, immunostaining with anti-Myc antibody and rhodamine-labeled phalloidin revealed that the expressed Myc-wtMYOT, Myc-mMYOT S60C, and Myc-mMYOT R405K did not form abnormal protein aggregations, and they localized at actin stress fibers (Figure 2). Expression of mMYOT did not affect differentiation of C2C12 cells (data not shown).

Accumulation of Myotilin after Electroporation

To investigate the roles of mutant myotilin, we performed *in vivo* electroporation to express Myc-wtMYOT or Myc-mMYOT (S60C or R405K) in mouse TA muscles. At 7 and 14 days after electroporation, Myc-positive granules with diameters >1 μm were observed in Myc-tagged myotilin-expressing myofibers (Figure 3A). Compared with wtMYOT-expressing myofibers, mMYOT-expressing myofi-